

UNIVERSIDADE FEDERAL DE PELOTAS
Instituto de Física e Matemática
Programa de Pós-Graduação em Física



Dissertation

Tracer diffusion in crowded solutions of sticky polymers

Thiago Puccinelli Orlandi Nogueira

Pelotas, 2020

Thiago Puccinelli Orlandi Nogueira

Tracer diffusion in crowded solutions of sticky polymers

Master dissertation presented to the Graduate Program in Physics of the Institute of Physics and Mathematics of The Federal University of Pelotas as partial requirement to obtain the Master in Physics degree.

Supervisor: Prof. Dr. José Rafael Bordin

Co-supervisor: Prof. Dr. Francesco Piazza

Pelotas

2020

Universidade Federal de Pelotas / Sistema de Bibliotecas
Catalogação na Publicação

N778t Nogueira, Thiago Puccinelli Orlandi

Tracer diffusion in crowded solutions of sticky polymers / Thiago Puccinelli Orlandi Nogueira ; José Rafael Bordin, orientador ; Francesco Piazza, coorientador. — Pelotas, 2020.

61 f. : il.

Dissertação (Mestrado) — Programa de Pós-Graduação em Física, Instituto de Física e Matemática, Universidade Federal de Pelotas, 2020.

1. Difusão de macromoléculas. 2. Dinâmica de Langevin. 3. Anomalias de tipo água. 4. Afinidade entre tracers e polímeros. I. Bordin, José Rafael, orient. II. Piazza, Francesco, coorient. III. Título.

CDD : 539.6


Thiago Puccinelli Orlandi Nogueira

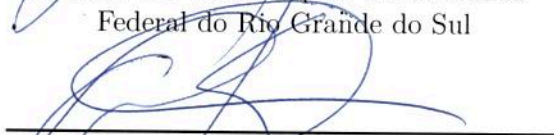
Tracer diffusion in crowded solutions of sticky polymers

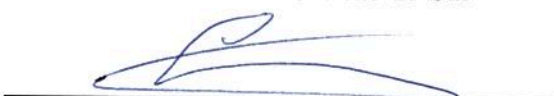
Dissertação aprovada, como requisito parcial, para obtenção do grau de Mestre em Física, Programa de Pós-Graduação em Física, Instituto de Física e Matemática, Universidade Federal de Pelotas.

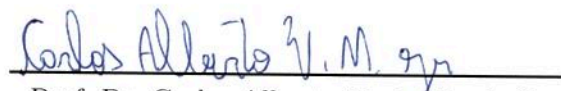
Data da Defesa: 21 de fevereiro de 2020

Banca examinadora:


Prof. Dr. José Rafael Bordin (Orientador)
Doutor em Ciências pela Universidade
Federal do Rio Grande do Sul


Prof. Dr. Mateus Henrique Köhler
Doutor em Ciências pela Universidade
Federal do Rio Grande do Sul


Prof. Dr. Alexandre Diehl
Doutor em Ciências pela Universidade
Federal do Rio Grande do Sul


Prof. Dr. Carlos Alberto V. de Moraes Jr
Doutor em Física pela Universidade Federal
de Santa Maria

Pelotas

2020

*À física por me permitir admirar, mesmo que de maneira singela,
os fenômenos da natureza.*

*Também a todos os futuros cientistas deste país
desejo levar a seguinte mensagem:*

*"Não desista do seu futuro,
independente das forças externas,
faça na ciência a sua resistência,
assim como uma mola resiste
entre dois brutos corpos..."*

Acknowledgements

I would like to thank the funding organization CAPES for the opportunity of having a masters scholarship during my masters. And CNPQ for providing technical equipments as computers for carrying out our simulations, which were valuable to our research and simulations. Nonetheless, I would like to thank the program *Pós-Graduação em Física* from UFPEL for the opportunity of having me for a master's thesis.

I would like to thank my former graduation supervisor, Prof. Dr. Hidembergue Ordozgoith da Frota, that was fundamental to my formation as a physicist, and gave me the chance to simulate the beggining part of our simulation results on his computer CLUSTER at UFAM.

In addition, I would like to thank my lab colleagues, Alexsandra Pereira, Ramon Carvalho and Tiago Braga for our jokes and scientific talks, that were of extreme importance to our research. Nonetheless, a thank you to Patricia Moreira, Celso Sena and Jean Reis that helped me in my adaptation in a new University, a new city, and a whole new life.

A special thank you to Íngrid Carvalho and Vitor Alano de Ataídes for having me living with them, and in this sense for helping me in my life adaptation to Pelotas, and even for the happy moments we had together. In addition another special thank you to Rafael Meireles for having a miraculous patience with me during the joyful moments I had with him during my masters.

Finally but not the least, I would like to thank my supervisors, Prof. Dr. José Rafael Bordin and Francesco Piazza, for giving me the opportunity to continue my scientific career, and for believing in me. Even when *dark clouds* fly over the Brazilian science.

“Não, o homem é vasto, vasto até demais; eu o faria mais estreito. Até o diabo sabe o que é isso, veja só! O que à mente parece desonra é tudo beleza para o coração. A beleza estará em Sodoma? Podes crer que é em Sodoma que ela está para a imensa maioria dos homens - conhecias ou não esse segredo? É horrível que a beleza seja uma coisa não só terrível, mas também misteriosa. Aí lutam o diabo e Deus, e o campo de batalha é o coração dos homens. Aliás, é a dor que ensina a gemer.”
(Fiódor Dostoiévski - Os Irmãos Karamázov)

Resumo

NOGUEIRA, Thiago Puccinelli Orlandi. **Diffusão de traçadores em soluções complexas de polímeros adsorventes**. 2020. 61 f. Dissertação (Mestrado em Física) - Programa de Pós-Graduação em Física, Instituto de Física e Matemática, Universidade Federal de Pelotas, Pelotas, 2020.

A difusão de macromoléculas em ambientes de geometria altamente confinada e ambientes povoados ainda é um campo em aberto na Física da Matéria Mole. O entendimento dos processos difusivos nestas condições é essencial para o completo entendimento de vários processos biológicos que possam ocorrer neste ambiente. Neste sentido, empregamos simulações em Dinâmica de Langevin em larga escala com o intuito de entender como as propriedades volumétricas de moléculas esféricas afetam a difusão das mesmas. Duas espécies de moléculas são utilizadas: uma é modelada através do potencial de Weeks-Chandler-Andersen, cuja natureza é puramente repulsiva, enquanto a segunda foi modelada como uma partícula interagindo segundo um potencial de caroço amolecido. Moléculas que interagem segundo este potencial podem ser proteínas globulares, colóides carregados e nanopartículas cobertas por polímeros. Estes sistemas são caracterizados pela presença de duas escalas no potencial de interação e podem apresentar anomalias de tipo água, em função da competição existente no potencial. Neste trabalho, estudamos as propriedades de estrutura e difusão destas duas espécies de moléculas em um meio povoado por polímeros. Analisamos como a afinidade entre moléculas e polímeros, além da densidade do sistema, afetam as propriedades de transporte e agregação de ambas espécies de moléculas. Curiosamente, a molécula, modelada através do potencial de Weeks-Chandler-Andersen, demonstrou um aumento na difusão, quando aumentamos sua fração de volume, de maneira similar como ocorre com anomalias da difusão de tipo água. Até seu mecanismo é similar ao que se observa em sistemas de tipo água. Discutimos nossos resultados nos baseando na competição nos potenciais de interação e na competição induzida pelo ambiente povoado.

Palavras-chaves: Difusão de macromoléculas; Dinâmica de Langevin; Anomalias de tipo água; Afinidade entre tracers e polímeros.

Abstract

NOGUEIRA, Thiago Puccinelli Orlandi. **Tracer diffusion in crowded solutions of sticky polymers**. 2020. 61 f. Dissertation (Master in Physics) - Programa de Pós-Graduação em Física, Instituto de Física e Matemática, Universidade Federal de Pelotas, Pelotas, 2020.

Macromolecular diffusion in strongly confined geometries and crowded environments remains as a open subject in soft matter Physics. Unveil the diffusion regimes in these conditions is essential for a complete understanding of several biological process. In this sense, we employ large scale Langevin Dynamics simulations to understand how the spherical tracer volumetric properties affects the diffusive properties. Two species of tracers are studied. One tracer particle is a standard soft-core particle modeled by the well known Weeks-Chandler-Andersen soft-core potential. The second is modeled as a Core-Softened particle. Core-softened macromolecules includes globular proteins, charged colloids and nanoparticles covered by polymeric brushes. These systems are characterized by the presence of two length scales in the interaction and can show waterlike anomalies regarding on the competition existent in the potential. In this work we study the diffusion and structure of these two tracer species in a polymeric crowded environment. We analyze how the tracer-polymer affinity and the system density affect the transport and aggregation properties. Surprisingly, the soft-core tracer particle shows a increase in the diffusion as we increase its volume occupancy – similar to the waterlike diffusion anomaly. Even the mechanism is similar to the observed in waterlike systems. We discuss our results based in the competitions in the interaction potentials and the competition induced by the crowded media.

Keywords: Macromolecular diffusion; Langevin Dynamics; Waterlike anomalies; Tracer-polymer affinity.

List of Figures

Figure 1	– (a) Massive simulation shows HIV capsid interacting with its environment. (b) Poliovirus (red) binding to glycoproteins on the cell surface and force their viral RNA inside. (c) <i>Escherichia coli</i> membrane cell. Source (a): https://phys.org/news/2017-07-massive-simulation-hiv-capsid-interacting.html Source (b) and (c): https://www.asbmb.org/asbmb-today/people/david-goodsell-the-master-of-mol-art	12
Figure 2	– (a) Total number of publications over the years, from the 1990’s to 2019, with the keyword ‘macromolecular crowding’ in the publications’ title. (b) Sum of times papers were cited over the years with the keyword ‘Macromolecular Crowding’ from the 1990’s to 2019. These data were collected using the Web of Science analysis research feature in https://www.webofknowledge.com/	13
Figure 3	– LJ potential profile. The arrow indicates the potential cutoff radius r_c . Source: The Authors.	17
Figure 4	– Weeks-Chandler-Andersen potential profile. Source: The Authors.	19
Figure 5	– Association plot of the WCA (green dashed line) and the FENE (red dashed line) potentials. The sum is represented by the solid line. R_0 is the chain maximum elongation distance given by the FENE potential. Source: The Authors.	20
Figure 6	– Core-Softened potential plot. With the parameters: $u_0 = 5.0$, $c_0 = 1.0$, e $r_0/\sigma = 0.7$. Inset: schematic representation of the particles undergoing this interaction with its core (first length scale at $r = 1.2\sigma$) and the soft corona (second length scale at $r \equiv 2\sigma$) and the force F multiplied by r as a function of r that shows a local minimum at $r = 1.2\sigma$ and another at $r = 2\sigma$. Source: The Authors.	21
Figure 7	– Standard <i>velocity</i> Verlet Molecular Dynamics algorithm schematic description. Source: The Authors	24
Figure 8	– Schematic discription of how to measure the RDF. The red particle is the reference particle, which a simple algorithm will count the neighboring particles in a shell at distance r and $r + dr$. Source: Wikipedia.	28

Figure 9 – Snapshots of the three-dimensional tracer-obstacle system used in our simulations. (a) System snapshot with only polymer obstacles at volume occupancy $\varphi_P = 0.1$ and (b) zoomed snapshot, in which we observe the presence of complex free spaces and voids. (c) Snapshot of the whole system, composed by the polymer obstacles in red and the tracer particles in green.	
Source: The Authors.	32
Figure 10 – Diffusion coefficient of tracer molecules, $D(\epsilon_{AB}, \phi_P)$, as a function of the polymer volume fraction ϕ_P for different values of the tracer-polymer affinity, ϵ_{AB} . (a) WCA tracers and (b) CS tracers. The diffusion coefficients are normalized to the $\epsilon_{AB} = 0$ value at the same values of ϕ_P to highlight the effect of the tracer-polymer affinity. Error bars are smaller than points.	
Source: The Authors.	35
Figure 11 – Diffusion coefficient of tracer molecules, $D(\epsilon_{AB}, \phi_P)$, as a function of the polymer volume fraction ϕ_P for different values of the tracer-polymer affinity, ϵ_{AB} . (a) WCA tracers and (b) CS tracers. The diffusion coefficients are normalized to the value at $\epsilon_{AB} = 0, \phi_P = 0$, to make the effect of varying both parameters explicit. Solid lines correspond to one-parameter fits to a model of diffusion in porous media, where the polymer matrix is modeled as an effective quenched suspension of hard spheres, see equation (4.1). Error bars are smaller than points.	
Source: The Authors.	36
Figure 12 – The polymer-tracer RDF $g_{AB}(r)$ for WCA (top) and (CS) particles for different values of the tracer-polymer affinity.	
Source: The Authors.	38
Figure 13 – The tracer-tracer RDF $g_{BB}(r)$ for WCA (top) and (CS) particles for different values of the tracer-polymer affinity.	
Source: The Authors.	39
Figure 14 – Diffusion coefficient of tracers normalized to the purely repulsive values $D(0, \phi_f)$ as a function of the fluid volume fraction ϕ_f for two values of ϵ_{AB} at fixed polymer volume fraction $\phi_P = 0.1$. Error bars are smaller than points.	
Source: The Authors.	41
Figure 15 – Polymer-tracer (a) and tracer-tracer (b) radial distribution functions at increasing values of the tracer packing fraction. The polymer matrix packing fraction is $\phi_P = 0.1$.	
Source: The Authors.	42

Contents

	Introduction	12
I	INTERACTION MODELS, COMPUTATIONAL METHODS FOR THE FLUID DIFFUSION STUDY AND SIMULATION DETAILS	16
1	INTERACTION MODELS	17
1.1	Lennard-Jones interaction	17
1.2	Weeks-Chandler-Andersen interaction	18
1.3	<i>Coarse-grained</i> interaction model for polymeric chains	18
1.4	Core-softened interaction	19
2	COMPUTATIONAL METHODS FOR THE FLUID DIFFUSION STUDY	22
2.1	Molecular Dynamics method	22
2.1.1	Standard algorithm	23
2.2	Equations of motion integration	23
2.3	Constant temperature simulation	25
2.3.1	Langevin dynamics	26
2.4	Diffusion theoretical model for fluids	26
2.4.1	Mean-squared displacement and diffusion coefficient	26
2.5	Radial distribution function	27
3	SIMULATION DETAILS	29
3.1	Reduced units	29
3.2	Computational methodology	30
3.3	The system	30
II	RESULTS, DISCUSSION AND CONCLUSION	33
4	RESULTS AND DISCUSSION	34
4.1	Diffusion and structure of the tracer fluid at different polymer packing fractions ϕ_P	34
4.2	The effect of self-crowding on diffusion	40
5	CONCLUSION	43

	BIBLIOGRAPHY	45
	ANNEX	51
	ANNEX A – LAMMPS SCRIPT	52
A.1	Variable	52
A.2	Simulation parameters	52
A.3	Data file for polymers	53
A.4	Tracers injection	55
A.5	Groups of molecules and interactions	55
A.6	Particle overlap	56
A.7	Integrator	57
A.8	Mean-squared displacement and radial distribution function evaluation	57
A.9	Run the simulation	58
A.10	LAMMPS full script	58

Introduction

The interior of biological cells, and almost every biological fluid medium, both extracellular and intracellular, has a common feature, which is the fact that they contain a high total concentration of macromolecules. But instead of calling this medium concentrated, it's more accurate to call it a crowded medium. Since, it's not a single macromolecular species that occurs to occupy the high concentration, but all taken together, the macromolecules occupy a significant fraction of the total volume (20-30%)^{1, 2}. For instance, in biological cells biomacromolecules occupy volume fractions going beyond 30% of its cytoplasmatic fluid^{3, 4, 5, 6, 7}. This complex and confined environment constitutes the condition known as macromolecular crowding, which involves non-specific interactions among macromolecular species due to excluded volume, van der Waals, electrostatic and hydrodynamic interactions⁸. This crowded environment may even affect the behavior of protein molecules. For instance, it was found that the macromolecular crowding promotes self-association of the Filamenting temperature-sensitive mutant Z protein (FtsZ) which is essential for cell division, and accelerates the rate of amyloid formation^{9, 10}. Also, experiments have shown that macromolecular crowding reduces the size of proteins even to volume fractions similar to that in cytosol, whereas DNA undergoes a coil-to-globule transition at very small volume fractions¹¹. Even, macromolecular crowding influences rates, equilibria and mechanism of biochemical reactions and the thermodynamics taking place inside the biological cells^{12, 2}. Figure 1 illustrates how the biological medium is crowded.

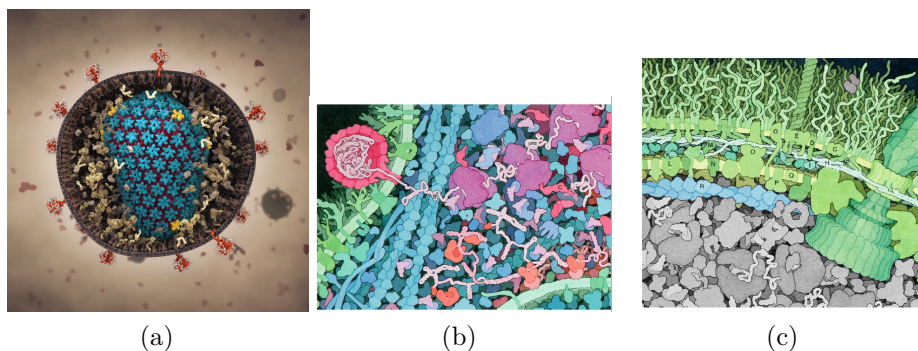


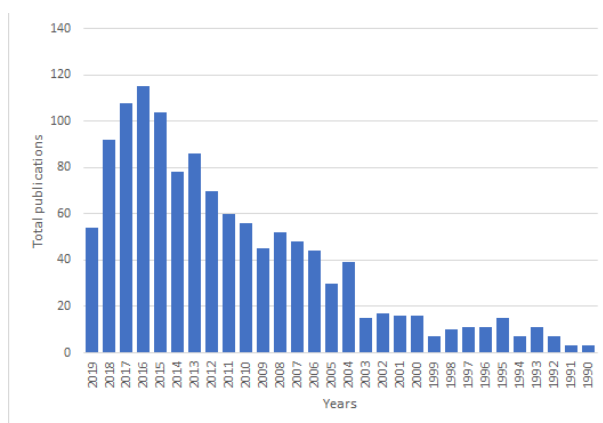
Figure 1 – (a) Massive simulation shows HIV capsid interacting with its environment. (b) Poliovirus (red) binding to glycoproteins on the cell surface and force their viral RNA inside. (c) *Escherichia coli* membrane cell.

Source (a): <https://phys.org/news/2017-07-massive-simulation-hiv-capsid-interacting.html>

Source (b) and (c): <https://www.asbmb.org/asbmb-today/people/david-goodsell-the-master-of-mol-art>

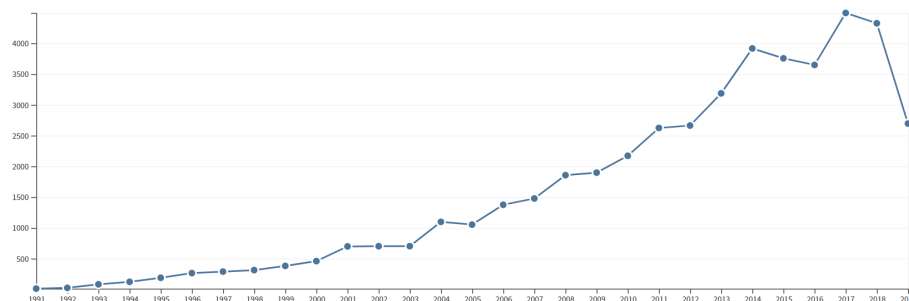
The scientific community since the 1990's has a growing interest in understanding

the macromolecular crowding, as we observe in figure 2 (a). This figure shows the total number of publications over the years from the 1990's to 2019. These publications had the keyword macromolecular crowding in their titles. As we can see there is an exponential growth from the 1990's until now. Nonetheless, when we look at the total of times a publication with the same keyword was cited (see figure 2 (b)), specifically between 2017 and 2018, the amount of citations reached more than 4000 times. This fuels even more our interest in understanding the influence of macromolecular crowding, for instance, in the diffusion processes of macromolecules.



(a)

Sum of Times Cited per Year



(b)

Figure 2 – (a) Total number of publications over the years, from the 1990's to 2019, with the keyword 'macromolecular crowding' in the publications' title. (b) Sum of times papers were cited over the years with the keyword 'Macromolecular Crowding' from the 1990's to 2019. These data were collected using the Web of Science analysis research feature in <https://www.webofknowledge.com/>.

Diffusion processes are well described by the traditional Fluid Mechanics for the cases of dilute mixtures in non-complex geometries. This is not the case of diffusion process in biological environment. Specially, it substantially alters the diffusion processes occurring inside these environments ^{1, 13}. Macromolecular diffusion and crowding influence on it are not fully comprehended by the scientific community, but efforts are underway to clarify this correlation ². Lately, experimental studies have been carried out to study macromolecular

diffusion in crowded media. *In vivo* experiments, such as fluorescent tracer introduced into a cell, allows a direct understanding of the macromolecular crowding. Unfortunately, the intrinsic differences between the different intracellular microenvironments make the interpretation of the results difficult⁸. In order to overcome this issue, *in vitro* experiments sought to recreate the crowded environment using highly concentrated polymer solutions, as dextran or ficoll^{14, 15}. After, spectroscopic techniques are employed to study the fluorescent macromolecules dynamics¹⁶, mainly Fluorescent Correlation Spectroscopy (FCS)¹⁴ and Fluorescent Recovery After Photobleaching (FRAP)¹⁵. In addition to these experimental findings, the use of computational simulations has become indispensable, since it provides a highly controlled environment⁸. Therefore, the comparison between computational and experimental analysis provides a better understanding on the factors governing macromolecular diffusion in crowded environments.

In this sense, different computational techniques have been applied from Monte Carlo simulations^{17, 18} and Brownian Dynamics (BD)^{19, 20, 21, 22, 23, 24, 25} to Molecular Dynamics simulation^{23, 26, 27}, and from Phase Fields applications in biological systems^{28, 29} to Lattice Boltzmann^{30, 31, 32}. Generally, macromolecules tends to have flexible structures. Therefore, when two macromolecules approach each other their branches can become entangled and non-specific attractive and/or repulsive interactions take place. This must be closely linked to macromolecular diffusion in crowded media. Thus, the need of models going beyond the hard-core spheres are necessary³³ to not lose the conformational dynamic behavior of macromolecules. Core-softened colloids and proteins are characterized by the presence of two length scales in the interaction, usually a short range attraction and a long range repulsion^{34, 35}. The repulsion can be caused by a soft shell, as in the case of polymeric brushes^{36, 37, 38, 39, 40} and star-polymers^{41, 42, 43, 44}, or by electrostatic repulsion in charged colloids, macromolecules, lysozyme and spherical proteins^{17, 35, 45, 46}, while the attraction is caused by van der Waals forces or solvent effects^{47, 48}. These core-softened potentials have also been largely employed to study systems with waterlike anomalies^{17, 49, 50, 51} and the confinement effects in these anomalies^{52, 53, 54}. Once we are interested in the diffusion process, the diffusion anomaly is of special interest. For most materials the diffusion coefficient decreases when the pressure (or density) increases. However, anomalous materials as water⁵⁵, silicon⁵⁶ and silica⁵⁷ show diffusion anomaly, characterized by a maximum in the diffusion coefficient at constant temperature. Therefore, a question that arises is how the crowded media influences the diffusion of soft-core, core-softened and soft tracer particles immersed in a polymeric environment. Nonetheless, how the tracer's softness and geometry influence the diffusion as well.

To answer this question we divided our work in a main objective and a specific branch objective. In one way, our main objective is to understand how diffusion works in crowded media. In the other way, our specific objective is to understand how the difference between soft-core and core-softened softness influence the diffusion of such tracers in the

crowded media.

To proceed with these objectives, we employed large scale Langevin Dynamics simulations to understand how the tracer volumetric properties affects the diffusive properties. Two species of tracers are studied. One tracer particle is a standard soft-core particle modeled by the well known Weeks-Chandler-Andersen (WCA) purely repulsive potential, which does not have competition since it has only one length scale. The second is modeled as a core-softened particle (CS), which shows a competition due its hard core-soft corona characteristic. In order to mimic the macromolecular crowding we inject these tracer molecules in a complex polymeric solution given by a coarse-grained model ⁵⁸. Our goal is to analyze the diffusion and the structure of these two molecule species in the polymeric media, analyzing how the tracer-polymer affinity and density affects the transport and aggregation properties.

This master's dissertation was divided in two parts: in the first one we describe the interaction models (Chapter 1), the computational methods for the fluid diffusion study (Chapter 2), the simulation details used in our research (Chapter 3) and the description of our proposed study system (Chapter 3.3); in the second part we present our results and discussion (Chapter 4), followed by the master's dissertation conclusion and future work ideas (Chapter 5). Finally, we present in the Annex A the LAMMPS full script with some coding information extracted from LAMMPS manual about the commands used in the full script.

Part I

Interaction models, computational methods for
the fluid diffusion study and simulation details

1 Interaction models

In this chapter, we will discuss the most used interaction models between particles in fluid simulations, which are used in this work. Firstly, we will present the Lennard-Jones potential (LJ), followed by the Weeks-Chandler-Andersen potential (WCA), the association of this potential and the Finitely Extensible Nonlinear Elastic potential (FENE) for the construction of polymer chains, which will form the complex media in our simulations. Add to this, we will present the Core-Softened potential (CS).

1.1 Lennard-Jones interaction

The Lennard-Jones interaction (LJ) is a mathematical model proposed to describe the interaction between pair of neutral atoms or molecules. This potential was firstly proposed by John Lennard Jones in 1924 ⁵⁹, namely

$$U_{\text{LJ}}(r) = \begin{cases} 4\epsilon_{AB} \left[\left(\frac{\sigma}{r} \right)^{12} - \left(\frac{\sigma}{r} \right)^6 \right], & r \leq r_c, \\ 0, & r \geq r_c, \end{cases} \quad (1.1)$$

where ϵ is the well depth, σ is the distance where the potential is equal to zero, and r_c is the cutoff radius. The LJ potential profile is illustrated in Figure 3. This potential is a function

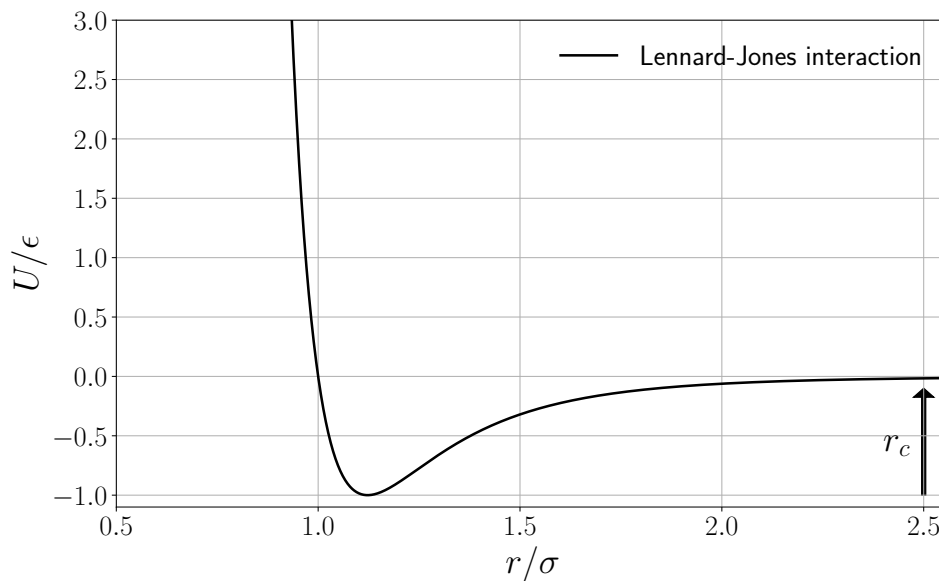


Figure 3 – LJ potential profile. The arrow indicates the potential cutoff radius r_c .
Source: The Authors.

of the distance between the centers of two particles. When two non-bonding particles

are a much greater distance than r_c apart, the possibility of them coming together and interacting is minimal. Their bonding potential energy is considered to be zero. However, as the distance of separation decreases, the probability of interaction increases. The particles come closer together until they reach a region of separation where the two particles become bound; their bonding potential energy decreases from zero to a negative quantity. While the particles are bound, the distance between their centers continue to decrease until the particles reach an equilibrium, specified by the separation distance at which the minimum potential energy is reached ($-\epsilon$). If the two bound particles are further pressed together, past their equilibrium distance, repulsion begins to occur. In terms of computational efficiency, it is common to choose a cutoff radius $r_c = 2.5\sigma$, which means that when two particles are separated by a distance larger than 2.5σ , their interaction will not be computed.

1.2 Weeks-Chandler-Andersen interaction

Another interaction model is a modification of the LJ potential, known as the Weeks-Chandler-Andersen potential (WCA) ⁶⁰, given by

$$U_{\text{WCA}}(r) = \begin{cases} 4\epsilon \left[\left(\frac{\sigma}{r}\right)^{12} - \left(\frac{\sigma}{r}\right)^6 + \frac{1}{4} \right], & r \leq r_c, \\ 0, & r \geq r_c, \end{cases} \quad (1.2)$$

where ϵ and σ are the characteristic energy and distance parameters, respectively; r_c is the cutoff radius. This potential exhibits only the repulsive part of the LJ potential. In this way, we cut it only in the distance where the potential is zero, $r_c = 2^{1/6}\sigma$. This potential profile is shown in Figure 4. This interaction has a factor $1/4$ in equation (1.2), which shifts it up positively by a factor ϵ . If this factor is considered to be zero and considering a cutoff radius $r_c = 2.5\sigma$, we would return to the well known LJ interaction. The analysis of this function is rather different from the late interaction, since we cut the potential where the energy is zero, $U = 0$. Therefore, the particles undergoing this interaction potential would feel only a strong repulsion, when their separation distance decreases from $r = 2^{1/6}\sigma$.

1.3 Coarse-grained interaction model for polymeric chains

For the generation of polymeric chains in molecular simulations, it is common to use a *coarse-grained* ^{58, 61} model, in which the polymer is treated as a collection of beads binded by springs. This model is an association of the WCA potential given by equation (1.2), and the Finitely Extensible Nonlinear Elastic potential (FENE), which

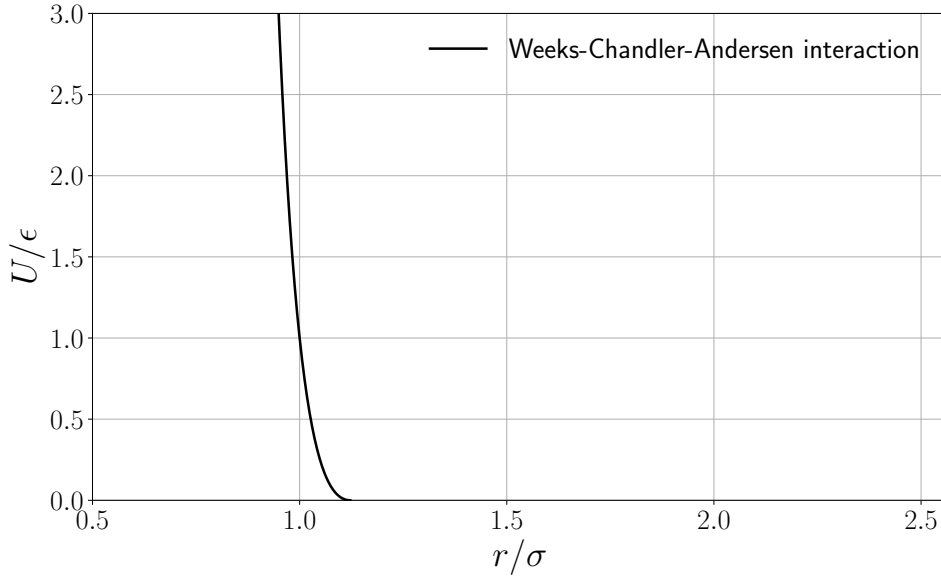


Figure 4 – Weeks-Chandler-Andersen potential profile.
Source: The Authors.

binds the beads as springs, according to

$$U_{\text{FENE}}(r) = \begin{cases} -0.5kR_0^2 \ln \left[1 - \left(\frac{r}{R_0} \right)^2 \right], & r \leq R_0, \\ \infty, & r \geq R_0, \end{cases} \quad (1.3)$$

where k is the elastic spring coefficient and R_0 is the maximum extent of the bond. This potential profile is shown in Figure 5. In this work, we used $k = 30\epsilon/\sigma^2$ e $R_0 = 1.5\sigma$. For the purpose of guiding the eyes, we represented in Figure 5 the WCA interaction by the green dashed line and the FENE interaction by the red dashed line, and then the sum of both potentials by the solid line. So one may see the contribution to this model of the WCA and FENE potentials. When the distance between the beads is $r = R_0$, they reach the maximum distance given by the FENE potential, then they are going to feel an attraction, but when they reach the distance of minimum energy given by the WCA potential, they will start to feel a strong repulsion. Therefore, the association of these potentials works as a harmonic potential, which keeps the beads binded. In this work, we used a collection of 50 beads to generate the polymer chain.

1.4 Core-softened interaction

The Core-Softened interaction (CS) is composed by a short-range attractive LJ potential and a repulsive gaussian term centered in r_0 , with depth u_0 and width c_0 , represented by the potential

$$U_{\text{CS}}(r) = 4\epsilon \left[\left(\frac{\sigma}{r} \right)^{12} - \left(\frac{\sigma}{r} \right)^6 \right] + u_0 \exp \left[-\frac{1}{c_0^2} \left(\frac{r - r_0}{\sigma} \right)^2 \right]. \quad (1.4)$$

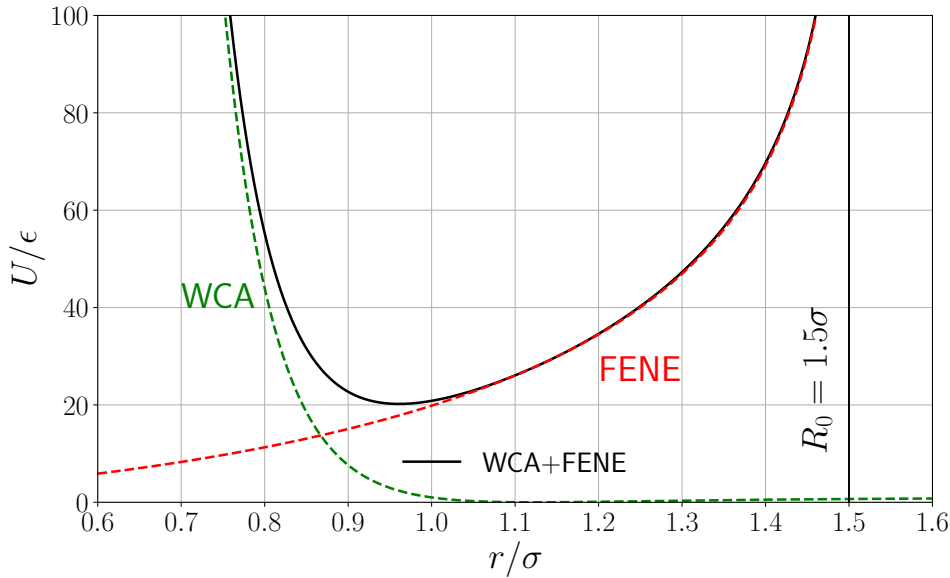


Figure 5 – Association plot of the WCA (green dashed line) and the FENE (red dashed line) potentials. The sum is represented by the solid line. R_0 is the chain maximum elongation distance given by the FENE potential. Source: The Authors.

This potential can be parametrized to have a ramplike shape, and was extensively applied to study systems with waterlike anomalies ^{49, 50, 62}. This potential profile is illustrated in Figure 6 with the parameters: $u_0 = 5.0$, $c_0 = 1.0$, $e r_0/\sigma = 0.7$. This interaction has two length scales: the first at $r \equiv 1.2\sigma$, where the forces has a local minimum, and another at $r \equiv 2\sigma$ (see graph inset in figure 6), where the fraction of imaginary modes of the instantaneous normal mode spectra has a local minimum ⁶³. The cutoff radius for the interaction is $r_c = 3.5\sigma$. The two length scales in this potential allow us to represent the interaction between hard core-soft shell colloids and proteins ^{64, 65}. The blue particle inset in figure 6 represents the particles interacting by this potential. Since this potential has two length scales, these scales are represented by the core (first length scale at $r \equiv 1.2\sigma$) and the soft corona (second length scale at $r \equiv 2\sigma$).

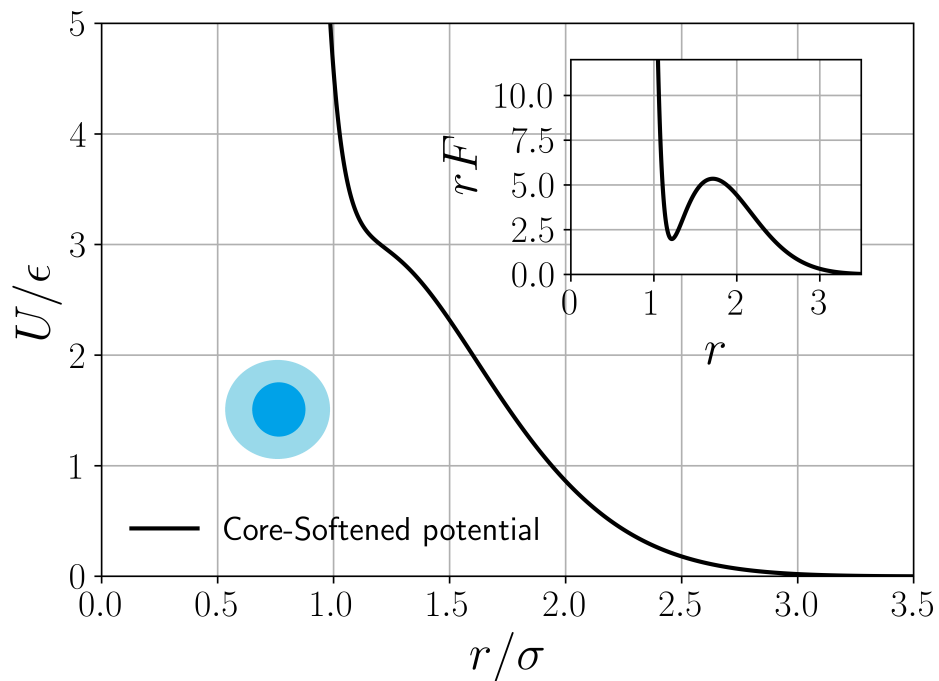


Figure 6 – Core-Softened potential plot. With the parameters: $u_0 = 5.0$, $c_0 = 1.0$, e , $r_0/\sigma = 0.7$. Inset: schematic representation of the particles undergoing this interaction with its core (first length scale at $r = 1.2\sigma$) and the soft corona (second length scale at $r \equiv 2\sigma$) and the force F multiplied by r as a function of r that shows a local minimum at $r = 1.2\sigma$ and another at $r = 2\sigma$. Source: The Authors.

2 Computational methods for the fluid diffusion study

In this chapter, we will review the main computational and theoretical methods for the fluid diffusion study. Nonetheless, the Molecular Dynamics (MD) method will be explored in this chapter, as the use of thermostats to keep the system temperature constant. For the use of such computational techniques, one must understand the theoretical background of the fluid diffusion, which is the classical Fick law for fluid dynamics. This theory will also be reviewed in this chapter. The Radial Distribution Function (RDF) for the structure analysis and the excess entropy calculation of the system will be presented as well. Since this work was carried out in the “*Large-scale Atomic/Molecular Massively Parallel Simulator*” package⁶⁶ (LAMMPS), this package will be presented as well.

2.1 Molecular Dynamics method

The main objective of this method is to study many-body systems, such as systems containing molecules, and then to analyze transport and equilibrium properties⁶⁷. For one to use this technique, one must solve the classical newtonian equations of motion for conservative systems, in the lagrangian form⁶⁸,

$$\frac{d}{dt} \left(\frac{\partial \mathcal{L}}{\partial \dot{q}_j} \right) - \frac{\partial \mathcal{L}}{\partial q_j} = 0, \quad (2.1)$$

where the lagrangian function $\mathcal{L}(\mathbf{q}, \dot{\mathbf{q}})$ is defined by the particles system kinetic (T) and potential (V) energies, namely

$$\mathcal{L} = T - V . \quad (2.2)$$

In this treatment, we are considering that the lagrangian function depends on the generalized coordinates q_j and their time derivatives \dot{q}_j . Doing so, and knowing the usual definitions of T and V added to the particles space positions defined in cartesian coordinates \mathbf{r}_i , the equation (2.1) becomes

$$m_i \ddot{\mathbf{r}}_i = \mathbf{f}_i , \quad (2.3)$$

where m_i is the i particle mass and

$$\mathbf{f}_i = \nabla_{\mathbf{r}_i} \mathcal{L} = -\nabla_{\mathbf{r}_i} V , \quad (2.4)$$

is the resultant force in the i particle given by the particle interactions with its surroundings. Therefore, the MD simulations implicates to solve the differential equation (2.3) for each particle in the studied system. In this way, one must solve for a three-dimensional system:

N equations of motion, where N is the number of particles in the system, e.g, for systems with one mole of molecules, one will need to solve $6,02 \times 10^{23}$ differential equations, which is impractical. This makes the use of computers and approximations very important.

2.1.1 Standard algorithm

The main methodology involving the MD software implementation is to set an initial system configuration with particles' positions and initial velocities for a time $t = 0$. This setting may be randomly distributed or following a gaussian distribution for the velocities, and for the particles' positions, they can be setted randomly as well or following a lattice distribution. Added to the initial setting, the computation of the interactions between these particles and its parameters are important too. After these steps, the program is ready to make simulation steps.

For the simulation, a final time and a step is setted. In this way, the program will compute a number of quantities during the simulation until it reaches the final step of simulation. The program will compute, e.g., the total force in each particle of the system due to the chosen interaction model. Afterwards, the equation of motion will be solved to generate the new particle positions and velocities, for a time t and $t + \delta t$, where δt is the simulation step. Some algorithms used for the equation of motion integration are presented in the next section. After the integration, normally a MD program computes the system energy, pressure, temperature, molecular self-diffusion, the radial distribution function and other sort of important data for analysis. When the program reaches the final step, it stops and print the data into outputs. A standard algorithm is illustrated in figure 7.

2.2 Equations of motion integration

In scientific literature one may find a number of algorithms that integrates the equations of motion. The *velocity* Verlet is the most used in MD simulations, and this method is used, e.g., in LAMMPS simulation package. To present this method, firstly, we have to present the Verlet algorithm, proposed by Loup Verlet in 1967^{69, 70}. The main goal is to write a Taylor expansion for the particle position $\mathbf{r}(t)$, for a future time $t + \delta t$ and for a past time $t - \delta t$. Defining $\mathbf{b} = d^3\mathbf{r}/dt^3$, one may write both expansions as

$$\begin{aligned}\mathbf{r}(t + \delta t) &= \mathbf{r}(t) + \mathbf{v}(t)\delta t + \frac{1}{2}\mathbf{a}(t)\delta t^2 + \frac{1}{6}\mathbf{b}(t)\delta t^3 + \mathcal{O}(\delta t^4) \\ \mathbf{r}(t - \delta t) &= \mathbf{r}(t) - \mathbf{v}(t)\delta t + \frac{1}{2}\mathbf{a}(t)\delta t^2 - \frac{1}{6}\mathbf{b}(t)\delta t^3 + \mathcal{O}(\delta t^4),\end{aligned}\quad (2.5)$$

respectively. Summing the above equations we have

$$\mathbf{r}(t + \delta t) = 2\mathbf{r}(t) - \mathbf{r}(t - \delta t) + \mathbf{a}(t)\delta t^2 + \mathcal{O}(\delta t^4). \quad (2.6)$$

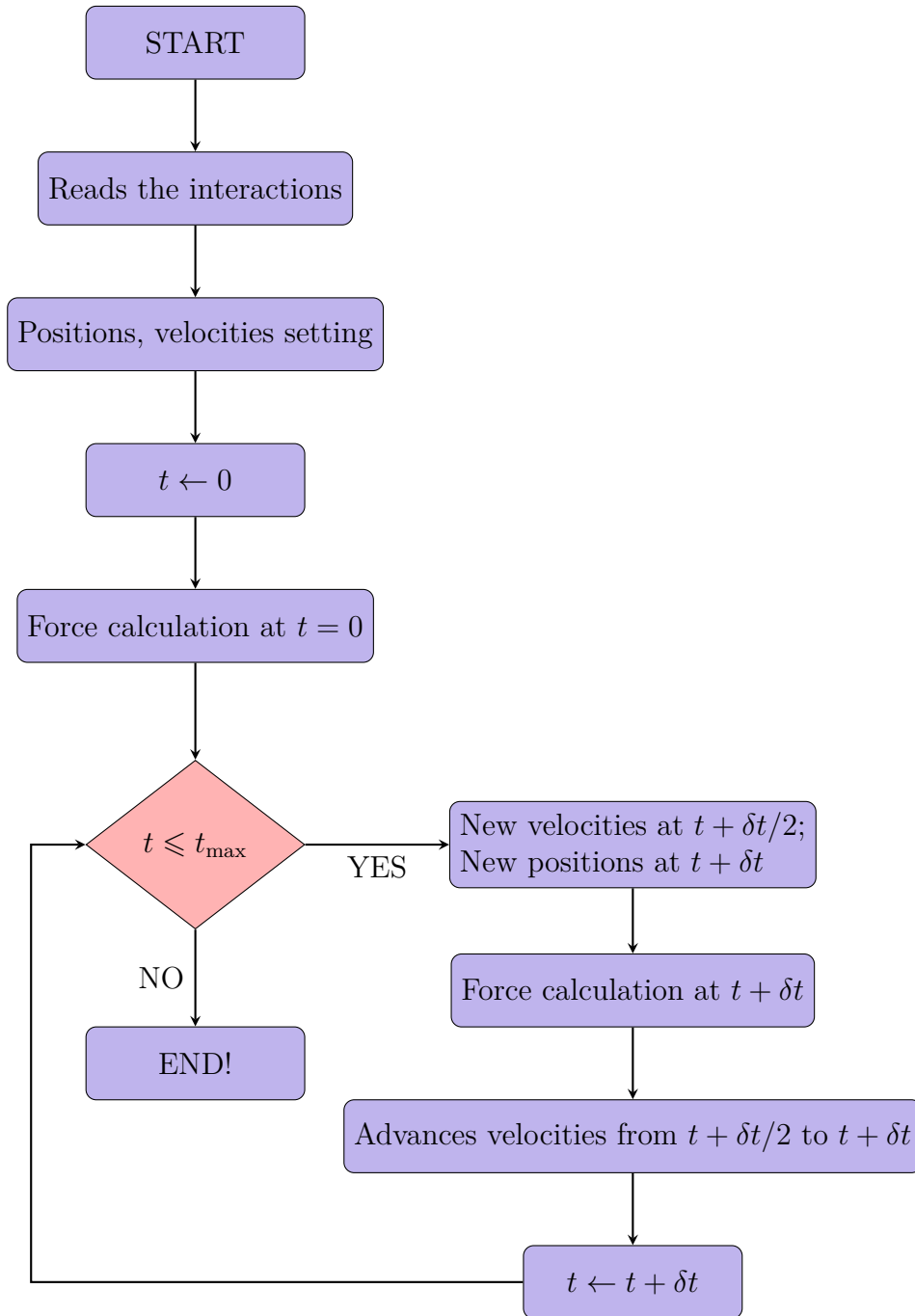


Figure 7 – Standard *velocity* Verlet Molecular Dynamics algorithm schematic description.
Source: The Authors

This is the traditional Verlet algorithm, with the order δt^4 uncertainty. Since we are integrating the Newton equations of motion, the particle acceleration $\mathbf{a}_i(t)$ is given by

$$\mathbf{a}_i(t) = -\frac{1}{m_i} \nabla U(r_{ij}), \quad (2.7)$$

where m_i is the i particle mass and $U(r_{ij})$ is the interaction potential between the particles i and j . The acceleration computation gives us the new particle positions. However, one may note that the new velocities are not computed simultaneously with the new positions.

Instead, the new velocities are computed using

$$\mathbf{v}(t) = \frac{\mathbf{r}(t + \delta t) - \mathbf{r}(t - \delta t)}{2\delta t}. \quad (2.8)$$

Therefore, the kinetic energy and the system temperature may be computed. Using this method, the new velocities computation generates an uncertainty in the order of δt^2 . This may generate significant fluctuations in the results computation. To avoid this, other algorithms were developed, such as the *velocity* Verlet⁷¹ that is represented by the Figure 7, which involves the simultaneously computation of the new positions and velocities.

This method follows two steps interspersed by the force computation. First knowing $\mathbf{a}(t)$ and $\mathbf{v}(t)$, the program computes the particle velocity for a time $t + \delta t/2$, given by

$$\mathbf{v}\left(t + \frac{1}{2}\delta t\right) = \mathbf{v}(t) + \frac{\delta t}{2}\mathbf{a}(t). \quad (2.9)$$

Then, the new positions are computed for a time $t + \delta t$, namely

$$\mathbf{r}(t + \delta t) = \mathbf{r}(t) + \mathbf{v}(t)\delta t + \frac{1}{2}\mathbf{a}(t)\delta t^2. \quad (2.10)$$

Therefore, the new accelerations are computed for a time $t + \delta t$ using equation (2.10), and also the new velocities,

$$\mathbf{v}(t + \delta t) = \mathbf{v}\left(t + \frac{1}{2}\delta t\right) + \frac{\delta t}{2}\mathbf{a}\left(t + \delta t\right). \quad (2.11)$$

Doing so, it is possible to minimize the errors in the equations of motion integration, since positions, velocities and accelerations are computed simultaneously for a time t .

2.3 Constant temperature simulation

The usual MD simulation keeps constant the number of particles N , the system volume V and the total system energy E . Totally isolated systems are not commonly found in nature, since the system interacts with its surroundings. From statistical mechanics point of view, it is known that systems in equilibrium with its surroundings or with a thermal reservoir, must be studied by the canonical *ensemble* theory. The simulations carried out for this matter are known as MD NVT .

When the system reaches the equilibrium, the particles velocities are distributed following the Maxwell-Boltzmann distribution, which means that the system temperature depends directly on the particles' average kinetic energy, and therefore on the particles' average velocities, namely

$$k_B T = m \langle v_j^2 \rangle, \quad (2.12)$$

where m is particle mass, v_j is the j -th particle velocity component, x , y and z in a three dimensional simulation, for instance, and k_B is the Boltzmann constant. By rescaling the

particles' velocities, we may control the system temperature. To accomplish this, we use thermostats. In scientific literature, one finds a number of thermostats, some of the most significant are: the Langevin and Andersen⁷² stochastic thermostats, and the Nosé-Hoover thermostat⁶⁷. Our simulations were carried out using the Langevin stochastic thermostat, which will be discussed in the next section.

2.3.1 Langevin dynamics

In each step of simulation under the Langevin Dynamics⁷² the particles undergoes the action of a viscosity force, proportional to each particles velocities and a viscosity coefficient. Added to this force, there is a stochastic force generated by a white noise, which simulates the effect of continuous collisions between the particles and a thermal reservoir. In this way, we may insert in the resultant force in each particle these two terms,

$$\mathbf{F}_R = -\nabla U - m\xi\mathbf{v}_i + \boldsymbol{\eta}_i(t), \quad (2.13)$$

where ξ is the friction coefficient and $\boldsymbol{\eta}$ is the stochastic force, generated by the Wiener process⁷³, responsible for the white noise. In this sense by the fluctuation-dissipation theorem, we might relate the noise and the system temperature using the distribution second momentum,

$$\langle \boldsymbol{\eta}_i(t)\boldsymbol{\eta}_j(t') \rangle = \delta_{ij}\delta(t-t')6k_B T\xi, \quad (2.14)$$

where δ_{ij} is the Kronecker delta, $\delta(t-t')$ is the Dirac delta, k_B is the Boltzmann constant, T is the system temperature and ξ is the friction coefficient with the thermostat. This relation indicates that the random forces are completely uncorrelated at different times. The first term in equation (2.13) corresponds to the interaction forces derived from the interaction potential. The Langevin Dynamics reduces to the Brownian Dynamics when $\nabla U = \mathbf{0}$, which means that there is no interaction among particles.

2.4 Diffusion theoretical model for fluids

In this section we will review one of the most studied analytical model for the diffusion in fluids, which is the analysis of the mean-squared displacement of the molecules in a MD simulation, and relate it to the diffusion coefficient.

2.4.1 Mean-squared displacement and diffusion coefficient

Diffusion is a process whereby an initially nonuniform concentration profile, for instance an ink drop in water, is smoothed in the absence of flow. Diffusion is caused by the molecular motion of the particles in the fluid⁶⁷. To analyze the dynamics of the particles

in a MD simulation, one should use the mean-squared displacement (MSD), which is a function of time, given by

$$\langle [\mathbf{r}(t) - \mathbf{r}(t_0)]^2 \rangle = \langle \Delta \mathbf{r}(t)^2 \rangle, \quad (2.15)$$

where $\mathbf{r}(t_0)$ and $\mathbf{r}(t)$ denote the position of a tracer molecule at a time t_0 and at a time t , respectively. The MSD is related to the diffusion coefficient, D , by the Einstein relation ⁷⁴,

$$D = \lim_{t \rightarrow \infty} \frac{\langle \Delta \mathbf{r}(t)^2 \rangle}{6t}. \quad (2.16)$$

This relation was first derived by Einstein ⁷⁴. While the diffusion coefficient D is a macroscopic property of the system, $\langle r^2(t) \rangle$ has a microscopic interpretation: it is the mean-squared distance over which the molecules have moved in a time interval t ⁶⁷. Therefore, this provides a method to compute D in computer simulations. For each past time in the simulation, one must measure the particles' traveled distance and plot the mean-squared displacement of these distances as a function of time.

In the case of disordered systems, there is a phenomena known as anomalous diffusion, that invalidates the relation (2.16). In this case the following relation works

$$\langle \Delta \mathbf{r}^2 \rangle = 2dDt^\alpha, \quad (2.17)$$

where d is the number of translational degrees of freedom and α is the anomalous diffusion exponent ⁷⁵. This exponent behavior is related to the particle diffusive behavior: that may be subdiffusive ($0 < \alpha < 1$), or superdiffusive ($1 < \alpha < 2$), or diffusive $\alpha = 1$, which leads back to the Einstein's equation (2.16).

2.5 Radial distribution function

To analyze the structure of fluids, one must make use of atomic distribution functions ⁷². The most simple one is the radial distribution function (RDF), given by

$$g(r_{ij}) = \frac{1}{\rho} \left\langle \frac{1}{N} \sum_{i=1}^N \sum_{j=1}^N \delta(\mathbf{r}_{ij} - \mathbf{r}_j + \mathbf{r}_i) \right\rangle, \quad (2.18)$$

where r_{ij} is the distance between atom i and atom j , ρ is the system density, N is the number of particles inside the system, and δ is the Dirac delta. In brief, the RDF provides us the probability of finding a pair of molecules at a distance r relative to the expected probability of a same density completely randomic distribution ⁷². Through this function analysis, one may confirm if the system is found to be in a gas, liquid or solid phase, given the long or short atomic organization shown in this function graph ⁷⁶. The schematic discription of how to compute this function is shown in Figure 8. Hence, we measure the probability of finding a particle at a distance r far from a reference particle relative

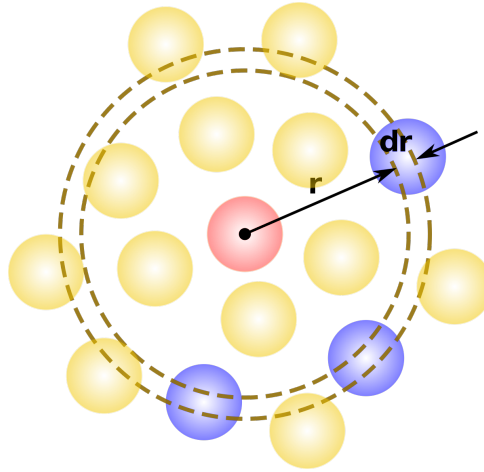


Figure 8 – Schematic description of how to measure the RDF. The red particle is the reference particle, which a simple algorithm will count the neighboring particles in a shell at distance r and $r + dr$.
Source: Wikipedia.

to an ideal gas phase distribution. The algorithm to compute this function involves the determination of how many particles are found inside the yellow shell (see again figure 8) at a distance r and $r + dr$ far from the reference particle. Looking at the figure, the red particle at the center is the reference particle, and the blue particle inside the shell will be accounted in the calculation, producing histograms with pairs, which will be normalized with respect to the case of an ideal gas.

3 Simulation details

In this chapter we will discuss the simulation details performed in this master's dissertation. Briefly, we will present the reduced units, describe the computational methodology, for instance the used time step in the simulations, how many steps were performed for system equilibration and for the production stage. Nevertheless, present the cluster infrastructure in which our simulations were carried out and discuss our proposed system studied in this master's dissertation.

3.1 Reduced units

In MD simulations, it's far convenient to express properties such as: temperature, density, pressure and many others in reduced units ⁶⁷. For instance, the fluid reduced particles density,

$$\rho^* \equiv \rho\sigma^3, \quad (3.1)$$

the time,

$$t^* \equiv t \underbrace{\left(\frac{\epsilon}{m\sigma^2} \right)^{1/2}}_{\tau} \equiv t\tau, \quad (3.2)$$

the temperature,

$$T^* \equiv \frac{k_B T}{\epsilon}, \quad (3.3)$$

the pressure,

$$p^* \equiv \frac{p\sigma^3}{\epsilon}, \quad (3.4)$$

the fluid diffusion coefficient,

$$D^* \equiv \frac{D(m/\epsilon)^{1/2}}{\sigma}. \quad (3.5)$$

This procedure facilitates, for instance, the computer computation tasks. Since it's difficult to deal with small constants, such as the Boltzmann constant, compared to higher values, which could lead to mathematical errors. Despite this feature, one more important reason for working with reduced units, is the fact that there are many possible combinations of density ρ , temperature T , and the LJ parameters: the well depth ϵ and the particle diameter σ , which corresponds to the same thermodynamic state ⁶⁷. Therefore, working with LJ simulations of liquid Argon at 60 K and density 840 kg/m³, is the same if we are dealing with Xenon at 112 K and density 1617 kg/m³, in reduced units. Both cases correspond to a state with density $\rho^* = 0.5$ and temperature $T^* = 0.5$.

3.2 Computational methodology

Our simulations were carried out using Langevin Dynamics, as described in Section 2.3.1. Hydrodynamics interactions were neglected. Since the system is in thermodynamic equilibrium, we do not expect that this will change the long-time behavior. The temperature was kept constant at $T^* = 4.45$. Such high temperature was chosen to ensure that the system is fluid even at high fluid densities.

The time step used in the simulations was $\delta t^* = 0.001$, and periodic boundary conditions were applied in the three directions, which means that if one particle crosses one side of the box, another particle is injected at the same spot but on the opposite box side. We performed 1×10^6 steps to equilibrate the system. These steps were, then, followed by 1×10^7 steps for the production stage. To ensure that the system has reached equilibrium, the kinetic and potential energy were analyzed as a function of time. System snapshots were also used to verify the equilibration. All simulations were carried out using LAMMPS MD software⁶⁶, which is a classical molecular dynamics code. This package is distributed as an open source code under the terms of the GPL. It runs on single processors or in parallel using message-passing techniques and a spatial-decomposition of the simulation domain. It was firstly presented by S. Plimpton in 1995 as a fast parallel algorithm for short-range molecular dynamics. At the present day, LAMMPS is developed by Sandia National Laboratories in the US Department of Energy in USA.

To obtain good statistics for our results, five independent simulations were used to produce our data. In each of these simulations, the polymers chains were firstly injected and we let them relax at random positions. In this way, for the five configurations, these polymers chains were not at the same positions. These simulations were runned in SATOLEP cluster in Universidade Federal de Pelotas.

3.3 The system

Since in biological cells biomacromolecules occupy volume fractions going beyond 30% of its cytoplasmatic fluid, this complex and confined environment is of our special interest in the study of molecular diffusion process inside these environments. In this sense, our objective is to study how the crowded media influences the diffusion of soft-core and core-softened tracer particles immersed in a complex media.

To simulate the above system, we sought to create the crowded media by injecting polymer chains in a simulation box and we let them relax to ensure that they are at random positions as shown in figure 9 (a). These polymers were modeled by a *coarse-grained* model, described in Section 1.3; for the molecule tracers, the soft-core species was modeled as WCA tracer, as described in Section 1.2; the core-softened species was modeled as a

CS tracer, as described in Section 1.4; the interaction between tracers and polymers was modeled with LJ interaction, as described in Section 1.1. The full picture of our proposed system is shown in figure 9 (c).

In our simulations, the packing fraction is defined as $\phi = Nv/L^3$, where L is the simulation box side, v is the single particle volume and N is the number of particles. Hence, we followed two strategies to tackle the crowded media influence on the molecules diffusion processes: first, we fixed the fluid packing fraction $\phi_f = 0.1$ and varied the polymer packing fraction ϕ_P from 0.001 up to 0.1; second, we did the way around, which was keeping $\phi_P = 0.1$ and varied ϕ_f from 0.1 up to 0.4. This enable us to study the effect of tracer and polymer crowding. In both strategies, we sought to analyze the diffusion and the structure of these two molecule species in the complex polymeric solution. Thus, analyzing how the tracer-polymer affinity, ϵ_{AB} (see equation 1.1), and density affects the transport and aggregation properties related to the case of an excluded volume, which means that $\epsilon_{AB} = 0$. In these simulations, the crowding media, the polymer network, was treated as rigid obstacles to the fluid diffusion, which means that they did not move during the results production stage in the MD simulation. It is important to note that, since we have done five independent simulations to obtain good statistics, in each of these simulations, the polymers chains relaxed to ensure that they were at random positions. In this way, we have five independent polymer chains configurations.

In order to exemplify how we implement the above description into a LAMMPS script code, for instance how we inject the polymers matrix and tracers into the simulation box, how we minimize the energy to avoid particles overlap, and how we insert particles interaction, one shall find these methods described in Annex A.

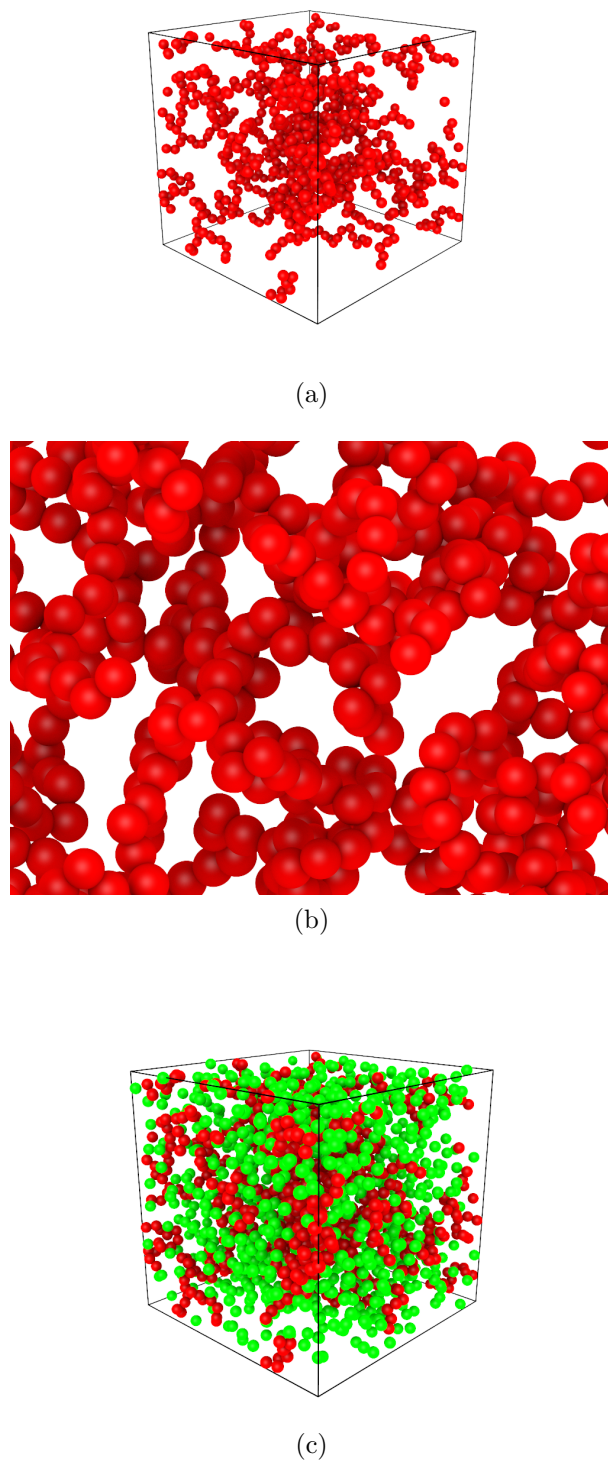


Figure 9 – Snapshots of the three-dimensional tracer-obstacle system used in our simulations. (a) System snapshot with only polymer obstacles at volume occupancy $\varphi_P = 0.1$ and (b) zoomed snapshot, in which we observe the presence of complex free spaces and voids. (c) Snapshot of the whole system, composed by the polymer obstacles in red and the tracer particles in green.

Source: The Authors.

Part II

Results, discussion and conclusion

4 Results and discussion

In this chapter, we will present our results and discussion. Since we followed two strategies to tackle the study of the effect of tracer and polymer crowding in the tracer molecules diffusion processes as described in Chapter 3.3: the first set of simulations refers to a fluid of tracers whose volume fraction was fixed at $\varphi = 0.1$ and immersed in a polymer matrix that occupies increasing fractions of the available volume; the second set of simulations, we varied the packing fraction of the tracers while keeping the crowding polymer matrix at $\varphi_P = 0.1$. In both cases, we considered both kinds of tracer-tracer interactions, namely single-length scale (WCA) and double-length scale (CS), and progressively increased the strength of the tracer-polymer interaction, ϵ_{AB} , from zero.

4.1 Diffusion and structure of the tracer fluid at different polymer packing fractions ϕ_P

The results of our simulations are illustrated in figure 10 and figure 11, where we chose two different ways to normalize the data. The effect of the tracer-polymer affinity ϵ_{AB} is best singled out by normalizing the measured diffusion coefficient through $D(0, \phi_P)$. Each point in the plot then quantifies the reduction in mobility caused by the tracer-crowder attractive interaction irrespective of the additional reduction due to crowding, i.e. excluded-volume. The first observation is that, surprisingly, a moderate attractive interaction seems to have no effect on the tracer mobility (circles in the upper panels). Increasing the strength of the tracer-polymer interaction beyond the value $\epsilon_{AB} = \epsilon$, that is, the typical repulsive energy at the monomer-tracer contact distance, tracer mobility appears progressively more and more hindered. In other words, a crowded environment that is also somewhat *sticky* causes more hindrance to tracer diffusion. This effect is larger the more crowded the environment, with $D(\epsilon, \phi_P)/D(\epsilon = 0, \phi_P)$ appearing to decrease linearly with the crowding packing fraction ϕ_P .

The second observation is that the presence of multiple length scales in the tracer-tracer interaction does not seem to induce noticeable differences in the way their mobility is shaped by the interaction with the environment. As a matter of fact, the reduction in diffusion for the WCA and CS fluid particles are very similar. While this may come to little surprise, as the tracer volume fraction is still on the low side ($\phi_f = 0.1$), we shall see that this observation on mobility is not mirrored by the corresponding static structure of the tracer fluid, which is characterized by different spatial correlations induced by the crowders that indeed appear to depend on the kind of tracer-tracer interaction.

In figure 11 we show the same data normalized in a different fashion, intended to

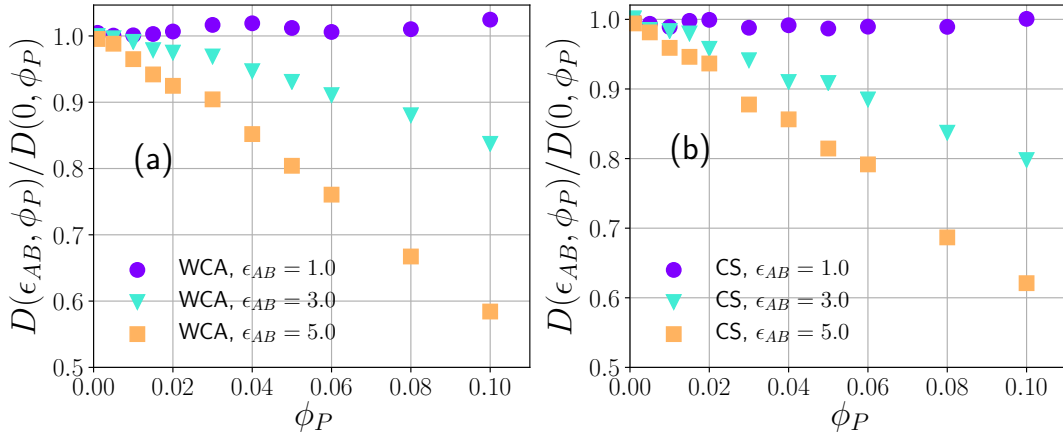


Figure 10 – Diffusion coefficient of tracer molecules, $D(\epsilon_{AB}, \phi_P)$, as a function of the polymer volume fraction ϕ_P for different values of the tracer-polymer affinity, ϵ_{AB} . (a) WCA tracers and (b) CS tracers. The diffusion coefficients are normalized to the $\epsilon_{AB} = 0$ value at the same values of ϕ_P to highlight the effect of the tracer-polymer affinity. Error bars are smaller than points. Source: The Authors.

highlight the combined action of crowder-tracer affinity and crowding volume fraction on diffusion. It can be clearly appreciated that an environment that is both crowded and somewhat *sticky* induces a substantial slowing down of the mobility. Tracers appear to loose between 60 and 70 % of their mobility at a polymer packing fraction as low as 10 % when the tracer-polymer attractive energy is between 3 to 5 times the typical energy ϵ . Again, this normalization does not reveal substantial differences in mobility ascribed to the kind of tracer-tracer interaction in the bulk.

It is instructive to compare our results with known predictions of diffusion in complex porous media. In such context, the ratio of the tracer diffusivity in the matrix to the Stokes-Einstein diffusivity D_0 in the pure suspending fluid is known as the so-called *tortuosity* τ . For a static matrix of spherical particles of diameter σ_1 with volume fraction ϕ , one has ⁷⁷

$$\frac{D(\phi)}{D_0} \equiv \tau(\phi) = (1 - \phi)^\nu [1 - \lambda_p(\phi)]^{a+b\lambda_p(\phi)} \quad (4.1)$$

where $\nu = 0.4$, $a = 4.2$, $b = 0.55$ and $\lambda_p(\phi)$ is the ratio of tracer particle diameter σ to the typical pore diameter $\sigma_p(\phi)$,

$$\lambda_p(\phi) \equiv \frac{\sigma}{\sigma_p(\phi)} = \left(\frac{\sigma}{\sigma_1}\right) \frac{3\phi}{1 - \phi} \quad (4.2)$$

It is interesting to inquire whether our polymer matrices behave as simple quenched suspensions of hard spheres by treating the diameter of such effective spheres σ_1 as an adjustable parameter. The fits shown in figure 11 reveal that our polymer matrices indeed behave as quenched suspensions of hard spheres over the whole range of parameters considered. More precisely, as the tracer-polymer interaction strength increases, the typical

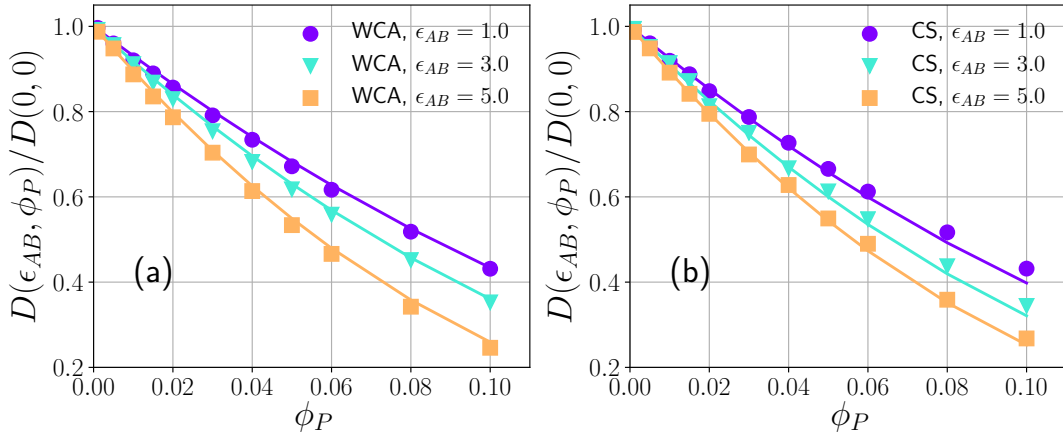


Figure 11 – Diffusion coefficient of tracer molecules, $D(\epsilon_{AB}, \phi_P)$, as a function of the polymer volume fraction ϕ_P for different values of the tracer-polymer affinity, ϵ_{AB} . (a) WCA tracers and (b) CS tracers. The diffusion coefficients are normalized to the value at $\epsilon_{AB} = 0, \phi_P = 0$, to make the effect of varying both parameters explicit. Solid lines correspond to one-parameter fits to a model of diffusion in porous media, where the polymer matrix is modeled as an effective quenched suspension of hard spheres, see equation (4.1). Error bars are smaller than points.

Source: The Authors.

ϵ_{AB}	WCA		CS	
	σ_1/σ	ϕ_P^c	σ_1/σ	ϕ_P^c
0.0	1.85 ± 0.02	0.381 ± 0.004	1.89 ± 0.02	0.386 ± 0.002
1.0	1.91 ± 0.02	0.389 ± 0.002	1.86 ± 0.03	0.383 ± 0.004
3.0	1.57 ± 0.01	0.343 ± 0.001	1.51 ± 0.02	0.335 ± 0.003
5.0	1.21 ± 0.01	0.287 ± 0.002	1.26 ± 0.01	0.296 ± 0.002

Table 1 – Best-fit values of the effective typical pore diameter σ_1 obtained by fitting equation (4.1) to our data over the whole range of polymer packing fraction ϕ_P . The corresponding void percolation thresholds ϕ_P^c computed from equation (4.3) are also reported.

effective pore size decreases, showing that *stickier* polymer matrices slow down tracers as quenched suspensions with smaller pores would do. This analogy also allows us to compute the equivalent void percolation threshold of the polymer matrix ϕ_P^c , that is, the critical packing fraction where the pore size equals the tracer size. From the condition $\lambda_p = 1$, equation (4.2) gives immediately

$$\phi_P^c = \frac{\sigma_1}{3\sigma + \sigma_1} \quad (4.3)$$

The best-fit values of the effective pore size and the corresponding percolation thresholds are reported in table 1.

The similar trends observed in the mobility of WCA and CS particles might still conceal some more conspicuous difference in the structural reorganization of the tracer

fluid induced by the sticky crowding matrices. In order to investigate this aspect, it is instructive to compute the radial distribution function (RDF), both for tracer-tracer pairs (BB) as well as for tracer-monomer pairs (AB).

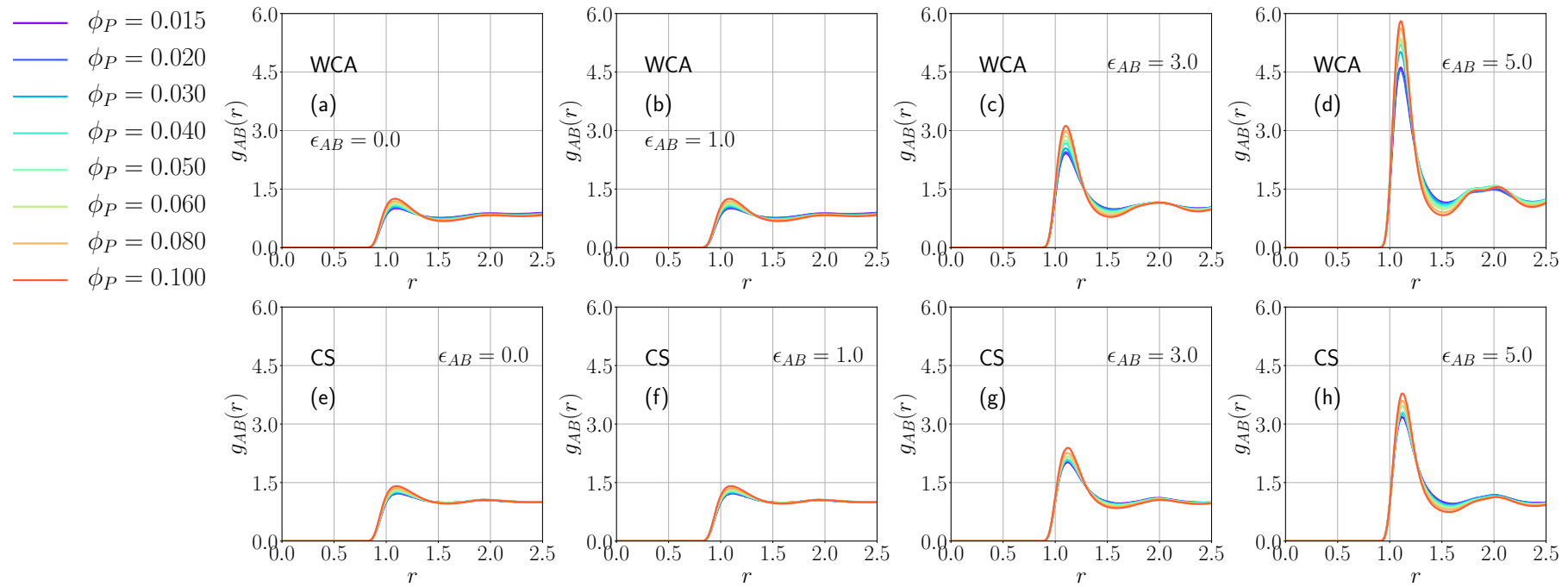


Figure 12 – The polymer-tracer RDF $g_{AB}(r)$ for WCA (top) and (CS) particles for different values of the tracer-polymer affinity.
Source: The Authors.

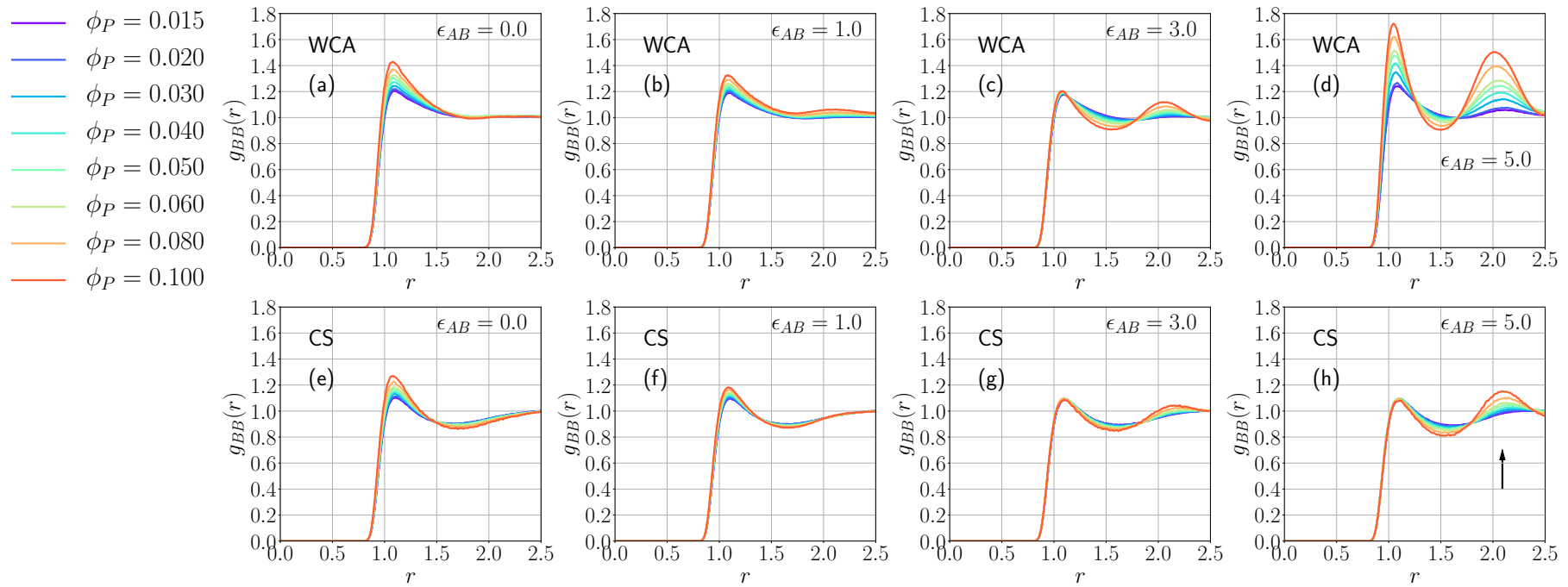


Figure 13 – The tracer-tracer RDF $g_{BB}(r)$ for WCA (top) and (CS) particles for different values of the tracer-polymer affinity.
Source: The Authors.

Figure 12 illustrates the behavior of the polymer-fluid RDF, $g_{AB}(r)$. Both kind of fluids appear to develop an increasing degree of structural organization in the vicinity of the polymer matrix as the polymer-tracer affinity increases beyond $\epsilon_{AB} = 1$. However, this analysis reveals that CS particles are much less prone to affinity-induced structural organization around the crowders. This observation can be interpreted as a direct result of the competition between different length scales in the repulsion between CS particles, which appears to induce some frustration in the spatial ordering of such tracers in the presence of crowding.

A direct inspection of the tracer-tracer RDFs $g_{BB}(r)$ (figure 13) confirms that structural ordering is globally hindered in the CS fluid. Interestingly WCA particles get more and more structured around each other at large values of ϵ_{AB} and the first and second coordination shells appear to become populated at essentially the same rate (see panel (d) in figure 13). By contrast, the dual length-scale repulsion of CS particles appears to essentially suppress any appreciable structuring in the first coordination shell, while the second shell becomes more and more populated, even if to a much lesser extent when compared to WCA particles (see arrow in panel (h) in figure 13).

4.2 The effect of self-crowding on diffusion

It is interesting to reverse the diffusion analysis illustrated above, where the fluid packing fraction was held fixed at $\phi_f = 0.1$, while we investigated the combined effect of ϵ_{AB} and the crowding volume occupancy, ϕ_P . In this section we analyze the results of simulations where the crowding density was fixed at the same moderate value, i.e. $\phi_P = 0.1$, while we let ϕ_f and ϵ_{AB} vary. In order to isolate the effect of the polymer-tracer affinity, we plot in figure 14 the diffusion coefficient of tracers $D(\epsilon_{AB}, \phi_f)$ normalized to the purely repulsive value at the same density, $D(0, \phi_f)$. As a first observation, it can be clearly appreciated that varying the fluid packing fraction (self-crowding) seems to have a less dramatic effect on diffusion than varying the crowding density. For low affinity, $\epsilon_{AB} = 1.0$, WCA and the CS tracers display an approximately constant diffusion coefficient, mirroring the corresponding trend observed in the reversed situation (see figure 10 (a) and (b)).

An interesting phenomenon is observed in the high-affinity case. When $\epsilon_{AB} = 5.0$, both tracer species display a water-like diffusion anomaly. It is clear from figure 14 that the diffusion constant increases as ϕ_f increase, reaches a maximum at $\phi_f \cong 0.2$ and then decreases again as the fluid density increases further. While for CS molecules this anomalous behavior is well known and directly ascribed to the dual-length repulsion^{49, 51}, it appears rather unexpected in the simple repulsive WCA fluid.

Some insight into this unexpected result can again be gathered by looking at the radial distribution functions at increasing values of ϕ_f in the high-affinity case (figure 15).

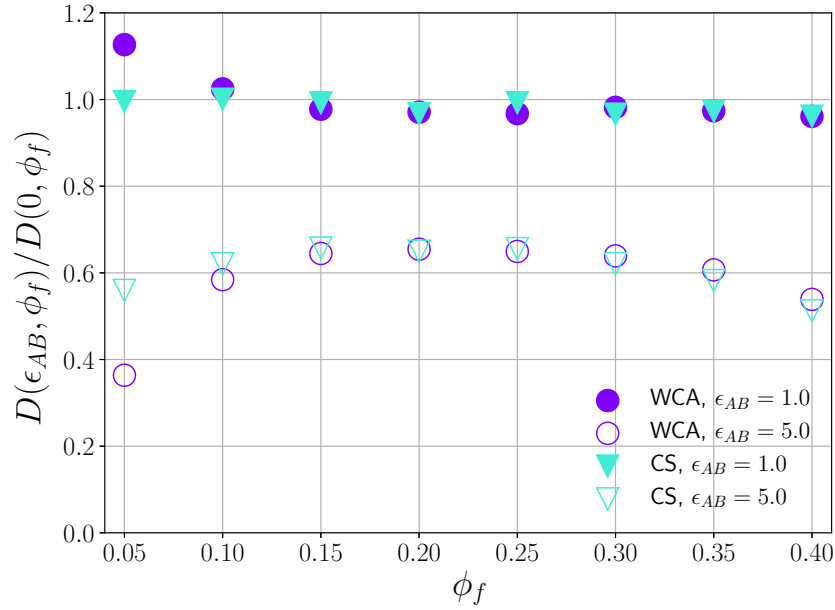


Figure 14 – Diffusion coefficient of tracers normalized to the purely repulsive values $D(0, \phi_f)$ as a function of the fluid volume fraction ϕ_f for two values of ϵ_{AB} at fixed polymer volume fraction $\phi_P = 0.1$. Error bars are smaller than points. Source: The Authors.

More precisely, it should be remarked that the effect of increasing the fluid density is to progressively lower the fraction of tracers adsorbed on the polymer matrix. This behavior is clearly illustrated by the decrease of both the first and second peaks in the polymer-tracer RDF, $g_{AB}(r)$. At the same time, while the polymer-tracer interface becomes less organized, the tracers start developing more short-range order. This is reflected by the increase of the first peak of the tracer-tracer RDF, $g_{BB}(r)$. Therefore, as we increase the fluid density, less and less tracers are adsorbed by the polymer matrix, thereby raising the number of unconstrained, fully mobile molecules in the bulk. However, increasing the fluid density further, the self-crowding effects become more prominent and the mobility of tracers starts decreasing as the fluid becomes more and more structured (see also the black arrows in figure 15).

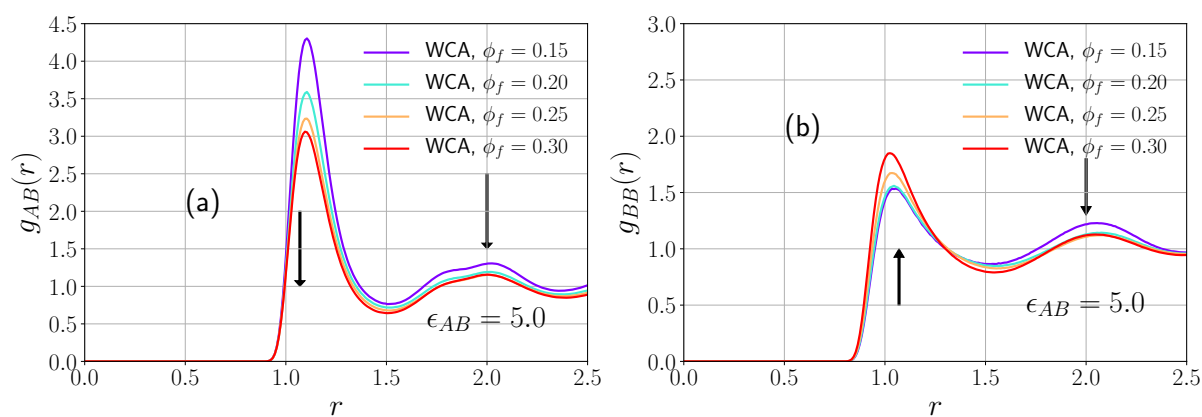


Figure 15 – Polymer-tracer (a) and tracer-tracer (b) radial distribution functions at increasing values of the tracer packing fraction. The polymer matrix packing fraction is $\phi_P = 0.1$.

Source: The Authors.

5 Conclusion

In this master's dissertation, we employed large-scale Langevin dynamics simulations to investigate the mobility of tracer particles diffusing in a static matrix consisting of quenched polymer chains of equal-sized monomers. The two main parameters varied were the volume fraction occupied by the polymer matrix and the strength of a short-range, non-specific attractive interaction causing tracer particles to spend longer time in the vicinity of the crowders. Furthermore, we focused on two types of tracer particles, characterized by different tracer-tracer repulsive interactions. In particular, we considered core-softened tracers (CS), characterized by a dual-length repulsive potential as compared to purely repulsive, shifted Lennard-Jones particles (WCA).

We found that excluded-volume interactions, i.e. crowding, reduce the tracer diffusion coefficient, all the more so the larger the polymer-tracer affinity. At the moderate tracer volume fraction considered in this paper ($\phi_f = 0.1$), we found no appreciable signature of the kind of tracer-tracer interactions in the measure diffusivity. The mobility of CS and WCA particles decreased with increasing crowding and increasing affinity following practically indistinguishable trends. In particular, we found that, for all the values of the attractive energy strength considered, the *sticky* crowding matrices behaved as porous media consisting of quenched suspensions of purely repulsive hard spheres, as gauged by fitting a tortuosity model to our data.

If the measured diffusion coefficients bore no blueprint of the underlying tracer-tracer interactions, the same was not true for static spatial correlations. In particular, for large crowding tracer affinity, the core-softened tracers showed a considerably lower propensity to structure around the polymers, whereas WCA particles showed substantial short- and intermediate-range order, increasing with the volume fraction of crowders.

In order to explore further the distinctive signature of the tracer-tracer repulsion in the high affinity case, we run a series of simulations at increasing density of tracers and intermediate crowding ($\phi_P = 0.1$) for $\epsilon_{AB} = 5$, comparing the measured diffusion coefficient to the zero affinity case. While we recovered the known water-like anomaly for CS particles, i.e. a non-monotonic trend of the diffusion coefficient as a function of the tracer density for high affinity, we found an even more pronounced anomaly of the same kind for the WCA particles. This kind of anomaly, which does not seem to be directly ascribed to dual-length repulsion, is more deeply, and likely more generally rooted in the competition between the confinement and the attraction exerted on tracers by the polymeric network. For dilute tracer fluids, an increase in self-crowding is seen to induce a progressive desorption of tracers from the polymer matrix, while the fluid gets more and

more structured in the bulk. The apparent result of this is that a little increase in ϕ_f from the very dilute case reduces $D(\epsilon_{AB} = 5, \phi_f)$ *less* than what observed in the zero-affinity case, i.e. less than $D(\epsilon_{AB} = 0, \phi_f)$. It is interesting to recall that a vast literature exists reporting a non-monotonic trend of the diffusion coefficient in the presence of crowding and tracer-crowder attractive interactions as the strength of the latter is increased. This scenario, also rooted in the competition between confinement and attraction, appears rather universal, from quenched-annealed mixtures of hard spheres⁷⁸, to ions in a charged polymer gel⁷⁹, nanoparticles in polymer melts⁸⁰ and simple hard-sphere like colloids⁸¹. However, despite the large body of work in this area, further work seems to be needed to gather a more comprehensive picture of tracer diffusion in the presence of crowded and attractive media in the regime where self-crowding effects become important.

Work ideas for the future

Since in this master's dissertation, we worked to understand how the softness of the tracers influences the diffusion in a crowded media, now we aim to investigate how the geometric feature of these tracers and of a soft particle should influence the diffusion in a crowded media. In this sense we will work with dimer particles diffusing in the same crowded media. Nonetheless, as we worked with a rigid crowded media, which means that the polymer network did not move during the simulation, we look forward to study how the molecules tracer diffusion might change, when the crowding media is no more rigid. For that case, we aim to parametrize our model to fit the experimental data obtained by Prof. Anand Yethiraj, from the Memorial University of Newfoundland, Canada. As well, we will keep the ongoing collaboration with Prof. Francesco Piazza.

Bibliography

- 1 ELLIS, R. J. Macromolecular crowding: obvious but underappreciated. *Trends in Biochemical Sciences*, Elsevier, v. 26, n. 10, p. 597–604, 2001.
- 2 RIVAS, G.; MINTON, A. P. Macromolecular crowding in vitro, in vivo, and in between. *Trends in Biochemical Sciences*, Elsevier, v. 41, n. 11, p. 970–981, 2016.
- 3 ZIMMERMAN, S. B.; TRACH, S. O. Estimation of macromolecule concentrations and excluded volume effects for the cytoplasm of escherichia coli. *Journal of Molecular Biology*, Elsevier, v. 222, n. 3, p. 599–620, 1991.
- 4 ZIMMERMAN, S. B.; MINTON, A. P. Macromolecular crowding: biochemical, biophysical, and physiological consequences. *Annual Review of Biophysics and Biomolecular Structure*, Annual Reviews 4139 El Camino Way, PO Box 10139, Palo Alto, CA 94303-0139, USA, v. 22, n. 1, p. 27–65, 1993.
- 5 ZHOU, H.-X. Protein folding and binding in confined spaces and in crowded solutions. *Journal of Molecular Recognition*, Wiley Online Library, v. 17, n. 5, p. 368–375, 2004.
- 6 ZHOU, H.-X.; RIVAS, G.; MINTON, A. P. Macromolecular crowding and confinement: biochemical, biophysical, and potential physiological consequences. *Annu. Rev. Biophys.*, Annual Reviews, v. 37, p. 375–397, 2008.
- 7 MCGUFFEE, S. R.; ELCOCK, A. H. Diffusion, crowding & protein stability in a dynamic molecular model of the bacterial cytoplasm. *PLoS Computational Biology*, Public Library of Science, v. 6, n. 3, p. e1000694, 2010.
- 8 BLANCO, P. M. et al. Macromolecular diffusion in crowded media beyond the hard-sphere model. *Soft Matter*, Royal Society of Chemistry, v. 14, n. 16, p. 3105–3114, 2018.
- 9 RIVAS, G. et al. Magnesium-induced linear self-association of the ftsz bacterial cell division protein monomer the primary steps for ftsz assembly. *Journal of Biological Chemistry*, ASBMB, v. 275, n. 16, p. 11740–11749, 2000.
- 10 HATTERS, D. M.; MINTON, A. P.; HOWLETT, G. J. Macromolecular crowding accelerates amyloid formation by human apolipoprotein c-ii. *Journal of Biological Chemistry*, ASBMB, v. 277, n. 10, p. 7824–7830, 2002.
- 11 KANG, H. et al. Effects of macromolecular crowding on the collapse of biopolymers. *Physical Review Letters*, APS, v. 114, n. 6, p. 068303, 2015.
- 12 MINTON, A. P. The influence of macromolecular crowding and macromolecular confinement on biochemical reactions in physiological media. *Journal of Biological Chemistry*, ASBMB, v. 276, n. 14, p. 10577–10580, 2001.
- 13 BALCELLS, C. et al. Macromolecular crowding effect upon in vitro enzyme kinetics: mixed activation–diffusion control of the oxidation of nadh by pyruvate catalyzed by lactate dehydrogenase. *The Journal of Physical Chemistry B*, ACS Publications, v. 118, n. 15, p. 4062–4068, 2014.

- 14 BANKS, D. S.; FRADIN, C. Anomalous diffusion of proteins due to molecular crowding. *Biophysical Journal*, Elsevier, v. 89, n. 5, p. 2960–2971, 2005.
- 15 PASTOR, I. et al. Diffusion of α -chymotrypsin in solution-crowded media. a fluorescence recovery after photobleaching study. *The Journal of Physical Chemistry B*, ACS Publications, v. 114, n. 11, p. 4028–4034, 2010.
- 16 DIX, J. A.; VERKMAN, A. Crowding effects on diffusion in solutions and cells. *Annu. Rev. Biophys.*, Annual Reviews, v. 37, p. 247–263, 2008.
- 17 VILASECA, E. et al. Diffusion in macromolecular crowded media: Monte carlo simulation of obstructed diffusion vs. frap experiments. *Theoretical Chemistry Accounts*, Springer, v. 128, n. 4-6, p. 795–805, 2011.
- 18 VILASECA, E. et al. New insights into diffusion in 3d crowded media by monte carlo simulations: effect of size, mobility and spatial distribution of obstacles. *Physical Chemistry Chemical Physics*, Royal Society of Chemistry, v. 13, n. 16, p. 7396–7407, 2011.
- 19 SUN, J.; WEINSTEIN, H. Toward realistic modeling of dynamic processes in cell signaling: Quantification of macromolecular crowding effects. *The Journal of Chemical Physics*, AIP, v. 127, n. 15, p. 10B617, 2007.
- 20 MEREGHETTI, P.; WADE, R. C. Atomic detail brownian dynamics simulations of concentrated protein solutions with a mean field treatment of hydrodynamic interactions. *The Journal of Physical Chemistry B*, ACS Publications, v. 116, n. 29, p. 8523–8533, 2012.
- 21 KONDRAT, S. et al. The effect of composition on diffusion of macromolecules in a crowded environment. *Physical Biology*, IOP Publishing, v. 12, n. 4, p. 046003, 2015.
- 22 SENTJABRSKAJA, T. et al. Anomalous dynamics of intruders in a crowded environment of mobile obstacles. *Nature Communications*, Nature Publishing Group, v. 7, p. 11133, 2016.
- 23 YU, I. et al. Biomolecular interactions modulate macromolecular structure and dynamics in atomistic model of a bacterial cytoplasm. *Elife*, eLife Sciences Publications Limited, v. 5, p. e19274, 2016.
- 24 BLANCO, P. M. et al. Brownian dynamics computational model of protein diffusion in crowded media with dextran macromolecules as obstacles. *Entropy*, Multidisciplinary Digital Publishing Institute, v. 19, n. 3, p. 105, 2017.
- 25 SMITH, S.; GRIMA, R. Fast simulation of brownian dynamics in a crowded environment. *The Journal of Chemical Physics*, AIP Publishing, v. 146, n. 2, p. 024105, 2017.
- 26 BUCCIARELLI, S. et al. Dramatic influence of patchy attractions on short-time protein diffusion under crowded conditions. *Science Advances*, American Association for the Advancement of Science, v. 2, n. 12, p. e1601432, 2016.
- 27 WANG, P.-h. et al. Influence of protein crowder size on hydration structure and dynamics in macromolecular crowding. *Chemical Physics Letters*, Elsevier, v. 671, p. 63–70, 2017.

- 28 GÜLTEKIN, O.; DAL, H.; HOLZAPFEL, G. A. Numerical aspects of anisotropic failure in soft biological tissues favor energy-based criteria: a rate-dependent anisotropic crack phase-field model. *Computer Methods in Applied Mechanics and Engineering*, Elsevier, v. 331, p. 23–52, 2018.
- 29 LÁZARO, G. R.; PAGONABARRAGA, I.; HERNÁNDEZ-MACHADO, A. Phase-field theories for mathematical modeling of biological membranes. *Chemistry and Physics of Lipids*, Elsevier, v. 185, p. 46–60, 2015.
- 30 MONTESSORI, A. et al. Multicomponent lattice boltzmann models for biological applications. In: *Numerical Methods and Advanced Simulation in Biomechanics and Biological Processes*. [S.l.]: Elsevier, 2018. p. 357–370.
- 31 NOËL, R. et al. Lattice boltzmann method for modelling of biological phenomena. In: *IEEE. 2017 25th European Signal Processing Conference (EUSIPCO)*. [S.l.], 2017. p. 2654–2658.
- 32 PAPAVALASSILIOU, D. et al. Lattice boltzmann methods for bioengineering applications. In: *Numerical Methods and Advanced Simulation in Biomechanics and Biological Processes*. [S.l.]: Elsevier, 2018. p. 415–429.
- 33 IRBÄCK, A.; MOHANTY, S. Protein folding/unfolding in the presence of interacting macromolecular crowders. *The European Physical Journal Special Topics*, Springer, v. 226, n. 4, p. 627–638, 2017.
- 34 STRADNER, A. et al. Equilibrium cluster formation in concentrated protein solutions and colloids. *Nature*, v. 432, p. 492–495, 2004.
- 35 SHUKLA, A. et al. Absence of equilibrium cluster phase in concentrated lysozyme solutions. *Proc. Natl. Acad. Sci. U.S.A.*, v. 105, p. 5075, 2008.
- 36 LAFITTE, T.; KUMAR, S. K.; PANAGIOTOULOS, A. Z. Self-assembly of polymer-grafted nanoparticles in thin films. *Soft Matter*, v. 10, p. 786, 2014.
- 37 CURK, T. et al. Nanoparticle organization in sandwiched polymer brushes. *Nano Letters*, v. 14, p. 2617–2622, 2014.
- 38 NIE, G. et al. Nanocomposites of polymer brush and inorganic nanoparticles: preparation, characterization and application. *Polym. Chem.*, v. 7, p. 753–769, 2016.
- 39 BEDROV, D.; AYYAGARI, C.; SMITH, G. D. Multiscale modeling of poly (ethylene oxide)- poly (propylene oxide)- poly (ethylene oxide) triblock copolymer micelles in aqueous solution. *Journal of Chemical Theory and Computation*, ACS Publications, v. 2, n. 3, p. 598–606, 2006.
- 40 BEDROV, D.; SMITH, G. D.; YOON, J. Structure and interactions in micellar solutions: molecular simulations of pluronic l64 aqueous solutions. *Langmuir*, ACS Publications, v. 23, n. 24, p. 12032–12041, 2007.
- 41 LIKOS, C. et al. Star polymers viewed as ultrasoft colloidal particles. *Physical Review Letters*, APS, v. 80, n. 20, p. 4450, 1998.

- 42 LOPPINET, B. et al. Dynamics of dense suspensions of star-like micelles with responsive fixed cores. *Macromolecular Chemistry and Physics*, Wiley Online Library, v. 206, n. 1, p. 163–172, 2005.
- 43 LIU, L.; OTTER, W. K. den; BRIELS, W. J. Coarse grain forces in star polymer melts. *Soft Matter*, Royal Society of Chemistry, v. 10, n. 39, p. 7874–7886, 2014.
- 44 LOCATELLI, E.; CAPONE, B.; LIKOS, C. N. Multiblob coarse-graining for mixtures of long polymers and soft colloids. *The Journal of Chemical Physics*, AIP Publishing, v. 145, n. 17, p. 174901, 2016.
- 45 QUESADA-PÉREZ, M. et al. Probing interaction forces in colloidal monolayers: Inversion of structural data. *J. Chem. Phys.*, v. 115, p. 10897, 2001.
- 46 CONTRERAS-ABURTO, C.; MÉNDEZ-ALCARAZ, J. M.; PRIEGO, R. C. neda. Structure and effective interactions in parallel monolayers of charged spherical colloids. *J. Chem. Phys.*, v. 132, p. 174111, 2010.
- 47 ALMARZA, N. G.; PEKALSKI, J.; CIACH, A. Periodic ordering of clusters and stripes in a two-dimensional lattice model. ii. results of monte carlo simulation. *The Journal of Chemical Physics*, AIP, v. 140, n. 16, p. 164708, 2014.
- 48 BORDIN, J. R. Distinct aggregation patterns and fluid porous phase in a 2d model for colloids with competitive interactions. *Physica A*, Elsevier, v. 495, p. 215–224, 2018.
- 49 OLIVEIRA, A. Barros de et al. Thermodynamic and dynamic anomalies for a three-dimensional isotropic core-softened potential. *The Journal of Chemical Physics*, AIP, v. 124, n. 8, p. 084505, 2006.
- 50 OLIVEIRA, A. B. de et al. Structural anomalies for a three dimensional isotropic core-softened potential. *The Journal of Chemical Physics*, AIP, v. 125, n. 12, p. 124503, 2006.
- 51 BORDIN, J. R.; BARBOSA, M. C. Waterlike anomalies in a two-dimensional core-softened potential. *Physical Review E*, APS, v. 97, n. 2, p. 022604, 2018.
- 52 KROTT, L. B. et al. Effects of confinement on anomalies and phase transitions of core-softened fluids. *J. Chem. Phys.*, v. 142, p. 134502, 2015.
- 53 KROTT, L.; BORDIN, J. R. Distinct dynamical and structural properties of a core-softened fluid when confined between fluctuating and fixed walls. *J. Chem. Phys.*, v. 139, p. 154502, 2013.
- 54 KROTT, L. B.; BORDIN, J. R.; BARBOSA, M. C. New structural anomaly induced by nanoconfinement. *J. Phys. Chem. B*, v. 119, p. 291–300, 2015.
- 55 NETZ, P. A. et al. Relation between structural and dynamical anomalies in supercooled water. *Physica A*, v. 314, p. 470, 2002.
- 56 MORISHITA, T. Anomalous diffusivity in supercooled liquid silicon under pressure. *Phys. Rev. E*, v. 72, p. 021201, 2005.
- 57 SASTRY, S.; ANGELL, C. A. Liquid-liquid phase transition in supercooled silicon. *Nature Mater.*, v. 2, p. 739–743, 2003.

- 58 KREMER, K.; GRETT, G. S. Dynamics of entangled linear polymer melts: A molecular-dynamics simulation. *The Journal of Chemical Physics*, AIP, v. 92, n. 8, p. 5057–5086, 1990.
- 59 JONES, J. E. On the determination of molecular fields.—ii. from the equation of state of a gas. *Proceedings of the Royal Society of London. Series A, Containing Papers of a Mathematical and Physical Character*, The Royal Society London, v. 106, n. 738, p. 463–477, 1924.
- 60 WEEKS, J. D.; CHANDLER, D.; ANDERSEN, H. C. Role of repulsive forces in determining the equilibrium structure of simple liquids. *The Journal of Chemical Physics*, American Institute of Physics, v. 54, n. 12, p. 5237–5247, 1971.
- 61 AUHL, R. et al. Equilibration of long chain polymer melts in computer simulations. *The Journal of Chemical Physics*, AIP, v. 119, n. 24, p. 12718–12728, 2003.
- 62 BORDIN, J. R.; BARBOSA, M. C. Waterlike anomalies in a two-dimensional core-softened potential. *Physical Review E*, APS, v. 97, n. 2, p. 022604, 2018.
- 63 OLIVEIRA, A. Barros de et al. Entropy, diffusivity and the energy landscape of a waterlike fluid. *The Journal of Chemical Physics*, AIP, v. 132, n. 23, p. 234509, 2010.
- 64 CIACH, A.; PEKALSKI, J. Exactly solvable model for self-assembly of hard core–soft shell particles at interfaces. *Soft Matter*, Royal Society of Chemistry, v. 13, n. 14, p. 2603–2608, 2017.
- 65 PATTABHIRAMAN, H.; GANTAPARA, A. P.; DIJKSTRA, M. On the stability of a quasicrystal and its crystalline approximant in a system of hard disks with a soft corona. *The Journal of Chemical Physics*, AIP Publishing, v. 143, n. 16, p. 164905, 2015.
- 66 PLIMPTON, S. Fast parallel algorithms for short-range molecular dynamics. *Journal of Computational Physics*, Elsevier, v. 117, n. 1, p. 1–19, 1995.
- 67 FRENKEL, D.; SMIT, B. *Understanding molecular simulation: from algorithms to applications*. [S.l.]: Elsevier, 2001. v. 1.
- 68 GOLDSTEIN, P.; POOLE, C. *Safko. Classical Mechanics*. [S.l.]: Addison Wesley, 2002.
- 69 VERLET, L. Computer "experiments" on classical fluids. i. thermodynamical properties of lennard-jones molecules. *Physical Review*, APS, v. 159, n. 1, p. 98, 1967.
- 70 VERLET, L. Computer "Experiments" on Classical Fluids. II. Equilibrium Correlation Functions. *Physical Review*, v. 165, n. 1, p. 201–214, jan 1968. ISSN 0031-899X.
- 71 SWOPE, W. C. et al. A computer simulation method for the calculation of equilibrium constants for the formation of physical clusters of molecules: Application to small water clusters. *The Journal of Chemical Physics*, American Institute of Physics, v. 76, n. 1, p. 637–649, jan 1982. ISSN 0021-9606.
- 72 ALLEN, M. P.; TILDESLEY, D. J. *Computer simulation of liquids*. [S.l.]: Oxford university press, 2017.

- 73 WIENER, N. Differential-Space. *Journal of Mathematics and Physics*, v. 2, n. 1-4, p. 131–174, oct 1923. ISSN 00971421.
- 74 EINSTEIN, A. Über die von der molekularkinetischen Theorie der Wärme geforderte Bewegung von in ruhenden Flüssigkeiten suspendierten Teilchen. *Annalen der Physik*, WILEY-VCH Verlag, v. 322, n. 8, p. 549–560, jan 1905. ISSN 00033804.
- 75 GHOSH, S. K. et al. Anomalous, non-Gaussian tracer diffusion in crowded two-dimensional environments. *New Journal of Physics*, IOP Publishing, v. 18, n. 1, 2016. ISSN 13672630.
- 76 GOODSTEIN, D. L. *States of matter*. [S.l.]: Dover, 1985. 500 p. ISBN 048664927X.
- 77 PEPPIN, S. S. L. Theory of tracer diffusion in concentrated hard-sphere suspensions. *Journal of Fluid Mechanics*, Cambridge University Press, v. 870, p. 1105–1126, jul 2019. ISSN 0022-1120.
- 78 PUTZEL, G. G.; TAGLIAZUCCHI, M.; SZLEIFER, I. Nonmonotonic diffusion of particles among larger attractive crowding spheres. *Physical Review Letters*, v. 113, n. 13, p. 138302, sep 2014. ISSN 0031-9007.
- 79 HOLMES, M. H. Nonlinear ionic diffusion through charged polymeric gels. *SIAM Journal on Applied Mathematics*, v. 50, n. 3, p. 839–852, 1990.
- 80 YAMAMOTO, U.; SCHWEIZER, K. S. Theory of nanoparticle diffusion in unentangled and entangled polymer melts. *Journal of Chemical Physics*, v. 135, p. 224902, 2011. ISSN 00219606.
- 81 PHAM, K. N. et al. Multiple glassy states in a simple model system. *Science*, American Association for the Advancement of Science, v. 296, n. 5565, p. 104–106, 2002. ISSN 0036-8075.

Annex

ANNEX A – LAMMPS script

In this annex, we shall describe the LAMMPS script used in our simulations. For instance, how to implement the polymer matrix; how to inject the tracers; how to set the interactions between types of particles; how LAMMPS minimizes the energy to avoid particles overlap; how to equilibrate the system; and how to measure properties in the production stage such as: the MSD, the RDF, the kinetic and potential energy. All these descriptions but not our full script were extracted from LAMMPS manual.

A.1 Variable

The variable command in LAMMPS assigns one or more strings to a variable name for evaluation later in the input script or during a simulation. For instance, one shall apply this command for setting the temperature, assign the number of particles, or the system density. This command is represented in the script in this way:

```
1    variable phif equal 0.1
```

In the above command line, we have setted the tracer fluid volume occupancy ϕ_f to a desired value 'equal' to 0.1. The variables are accessed by the command:

```
1    ${phif}
```

A.2 Simulation parameters

Before starting to simulate any system, LAMMPS needs to understand the environment in which the simulation will take place. In this sense, we need to set: the system dimension which is the dimensionality of the simulation that can be in three dimension or two; the style of units used for a simulation, which determines the units of all quantities specified in the input script and data file; the style of atoms to use in a simulation; the system boundaries, which can be periodic or not; the neighbor listing style, which affects the building of pairwise neighbor lists, all atom pairs within a neighbor cutoff distance equal to the their force cutoff plus the 'skin' distance are stored in that list. These parameters are illustrated in the following way

```
1    dimension 3
2    units    lj
3    atom_style    molecular
4    boundary          p p p
```

```
5 neighbor 3.0 multi
6 neigh_modify every 1 delay 0 check yes
```

the above script, we setted the system dimension to three; the units in ‘lj’, which means that all quantities are unitless, without loss of generality, LAMMPS sets the fundamental quantities mass, sigma, epsilon and the Boltzmann constant to one; the atom style by molecular that takes into account bonds, angles, dihedrals and impropers; we applied the periodic boundary conditions in the three directions (x,y,z) with ‘boundary p p p’; finally, the system neighboring list with its ‘skin’ equal to 3.0, that determines how often atoms migrate to new processors if the check option of the ‘neighbor modify’ command is set to yes.

A.3 Data file for polymers

In order to inject polymers into the system, one should generate a data file with the polymers information, such as: the number of monomers, the bonds, the angles, dihedrals, impropers, atom types, bond types, the box of simulation size and the position and velocities (of each monomer in the polymer chain). Unfortunately, LAMMPS does not have an embedded function to generate these kind of data file. Even, for polymers simulations. In this sense, scientists should make use of alternative codes for the polymer configuration wrote in lammeps standard data file format by following the above description. A illustrated data file format is presented bellow:

```
1 LAMMPS Description
2
3 5 atoms
4 4 bonds
5
6 1 atom types
7 1 bond types
8
9 -40 40 xlo xhi
10 -40 40 ylo yhi
11 -40 40 zlo zhi
12
13 Masses
14
15 1 1
16
17 Atoms # id mol type xu yu zu
```

```

18
19      1 1 2 -40.00000 0.00000 0.00000
20      2 1 1 -39.03500 0.00000 0.00000
21      3 1 1 -38.07000 0.00000 0.00000
22      4 1 1 -37.10500 0.00000 0.00000
23      5 1 1 -36.14000 0.00000 0.00000
24
25
26      Bonds
27
28      1 1 1 2
29      2 1 2 3
30      3 1 3 4
31      4 1 4 5

```

in the above data file, we have: 5 monomers in the polymer chain and 4 bonds between monomers that constitutes the whole chain with one monomer type and one bond type; and the simulation box size in the three directions (x , y and z); and the masses in ‘lj’ unities. These commands are illustrated as below:

```

1      5 atoms
2      4 bonds
3
4      1 atom types
5      1 bond types
6
7      -40 40 xlo xhi
8      -40 40 ylo yhi
9      -40 40 zlo zhi
10
11     Masses
12
13     1 1

```

Afterwards in the data file, one must describe all the atoms id, molecule id and molecular type followed by the atoms position. These description are illustrated bellow:

```

1      Atoms # id mol type xu yu zu
2
3      1 1 2 -40.00000 0.00000 0.00000
4      ...

```


Finally, we have to take into account the polymer chain bonds, which means which atom is bonded to which atom in the chain by the following way

```
1      Bonds
2
3      1 1 1 2
4      ...
```

The above command links the atoms bond in the chain, in this way: the first bond (1) of molecular type 1 links the first monomer (1) to the second monomer (2). With this data file complete, one shall insert in the LAMMPS script the polymer chain using the command bellow:

```
1      read_data polymer_chain.in
```

This command inserts the polymer chains, which are described in the polymer chain data file input, into the simulation box.

A.4 Tracers injection

To add the tracers in the simulation, we need to use this command:

```
1      region box block -40 40 -40 40 -40 40
2      create_atoms 2 random ${npart} 358723 box
```

the command ‘region’ defines a geometric region of space. And this region can be filled with atoms via the ‘create atoms’ command. In the above commands, we defined a region and filled with a number of atoms (variable $\{npart\}$) with type 2 in random positions, using a seed (358723) for a random number generator, into the ‘box’ of simulation.

A.5 Groups of molecules and interactions

To set the interactions between molecules, we need first to separate molecules types into groups and set the particles masses. This is done by the following commands:

```
1      mass      *          1
2
3      group obstacle type 1
4      group mobile  type 2
```

The ‘mass’ command sets for all kind of molecules (represented by the * symbol) the mass 1 (in ‘lj’ units). And then we group molecules by the command ‘group’ followed by the

group name and molecular type. Since we have injected the polymer with a data file before injecting the tracers, the polymer will have type 1, and then the tracers, the type 2. After this step, we need to set the particles interactions. For this script we are going to use WCA potential for tracer-tracer, tracer-polymer and polymer-polymer interactions, and the FENE bond for polymer-polymer. This setting is illustrated bellow:

```

1      #Weeks–Chandler–Anderson
2      pair_style          lj/cut  1.12246204830937
3      pair_coeff          * * 1.0  1.0  1.12246204830937
4      pair_modify        shift  yes
5
6      #FENE type bond
7      bond_style fene
8      bond_coeff 1 30.0  1.5  1.0  1.0
9      special_bonds fene

```

The command pair style sets the interaction, since we are modelling all the intermolecular interactions with the WCA potential, we need to use ‘lj/cut’ followed by its cutoff ‘ $2^{1/6}$ ’. Then, we set the pair coefficients for each pair of molecules, with $\epsilon = 1.0$, $\sigma = 1.0$ and $r_c = 2^{1/6}$. For the WCA case, one needs to modify it for LAMMPS, by shifting it upwards with the command pair modify shift yes. Finally, we specify the bonds in the polymer chain. In this case, we use the FENE bond, which is defined by the bond style fene, and its coefficients $k = 30.0$, $R_0 = 1.5$, $\epsilon = 1.0$ and $\sigma = 1.0$.

A.6 Particle overlap

To avoid particles overlap, we perform an energy minimization of the system, by iteratively adjusting atom coordinates. Iterations are terminated when one of the stopping criteria is satisfied. At that point the configuration will hopefully be in local potential energy minimum. The stopping criteria are: the total energy, the stopping force tolerance, the max iterations of the minimizer and its max number of force and energy evaluations, respectively. To implement the described minimization, we need to use the following command:

```

1      minimize 1.0e-4 1.0e-6 100 1000

```

For the first criterion, the specified energy tolerance is unitless; it is met when the energy change between successive iterations divided by the energy magnitude is less than or equal to the tolerance. For example, a setting of 1.0e-4 for the total energy means an energy tolerance of one part in 10^{-4} . For the second criterion, the specified force tolerance is in force units, since it is the length of the global force vector for all atoms, e.g. a vector of size

$3N$ for N atoms. Since many of the components will be near zero after minimization, one may think that this tolerance is an upper bound on the final force on any component of any atom. For example, a setting of $1.0\text{e-}4$ for this tolerance means no x, y and z component of force on any atom will be larger than $1.0\text{e-}4$ (in force units) after minimization. For the later tolerations, the first means the max iterations LAMMPS will perform the minimizer and the second the max number of force and energy evaluations.

A.7 Integrator

To use the equations of motion time integration in LAMMPS, one must use the ‘fix’ command added to the desired dynamics. Since we have performed Langevin Dynamics in our simulations, we have to use the Langevin thermostat added to a *NVE* time integration, the command is presented bellow:

```
1      fix integrator mobile nve
2      fix dynamics    mobile langevin ${temp} ${temp} 0.5 252352
```

Unlike the Nose-Hoover ‘fix nvt’ command performs thermostating and time integration, the ‘fix langevin’ does not perform time integration. It only modifies forces to effect thermostating. Thus one must use a separate time integration fix, like ‘fix nve’ to actually update the velocities and positions of atoms using modified forces. This ‘fix’ will need desired a temperature value, a damping factor and a seed, as seen above.

A.8 Mean-squared displacement and radial distribution function evaluation

To define a computation that calculates the mean-squared displacement of a group of atoms, including all effects due to atoms passing through peridic boundaries walls, one must use the following command:

```
1      compute 1 all msd
```

For the radial distribution function, one must define a computation that calculates this function and the coordination number for a group of particles. Both are calculated in histogram form by binning pairwise distances into a number of bins from 0.0 to the maximum force cutoff defined by the interactions. To define this computation, we need to use the following command:

```
1      compute 1 all rdf 256
```

A.9 Run the simulation

To run the simulation, we use the command ‘run’ added to a specified number of timesteps as shown below:

```
1      run 1000000
```

A.10 LAMMPS full script

Then, with all the above commands, we are able to perform the simulations used in this masters dissertation. The full script is shown bellow as an example:

```
1      #temperature in reduced units
2      variable temp equal 4.45
3
4      #number of obstacles to add
5      variable npart equal 40000
6
7      # Polymer pack frac
8      variable phi_poly equal 0.001
9
10     #set up basic simulation stuff
11     dimension 3
12     units      lj
13     atom_style molecular
14     boundary      p p p
15
16     #neighbor settings
17     neighbor 3.0 multi
18     neigh_modify every 1 delay 0 check yes
19
20     #read input configuraiton
21     read_data equil1.data
22
23     #add additional particles to box
24     region box block      -29.693150      29.693150  -29.693150
25     29.693150  -29.693150      29.693150
26     create_atoms 2 random ${npart} 358723 box
27
28     #all particles has mass 1
```

```
28     mass      *          1
29
30     #Type 1 is polymer. type 2 is fixed
31     group mobile type 2
32     group obstacle type 1
33
34     ##### INTERACTION #####
35     #Weeks-Chandler-Anderson + LJ POTENTIAL BETWEEN MOLECULES
        and Polymers
36     pair_style hybrid/overlay lj/cut 1.12246204830937 lj/cut
        2.5 lj/cut 1.12246204830937
37
38     # PAIR 1-1
39     pair_coeff      1 1 lj/cut 1 1.0 1.0 1.12246204830937
40     pair_modify      shift yes
41
42     # PAIR 1-2
43     pair_coeff      1 2 lj/cut 2 1.0 1.0 2.5
44
45
46     # PAIR 2-2
47     pair_coeff      2 2 lj/cut 3 1.0 1.0 1.12246204830937
48     pair_modify      shift yes
49
50     #FENE type bond
51     bond_style fene
52     bond_coeff 1 30.0 1.5 1.0 1.0
53     special_bonds fene
54
55     #####
56
57     #remove overlap between polymer and obstacles
58     minimize 1e-6 1e-6 10000 100000
59     reset_timestep 0
60
61
62     ##### SIMULATION INTEGRATOR #####
63     fix integrator mobile nve
64     fix dynamics      mobile langevin ${temp} ${temp} 1.0 252352
```

```
65
66
67   # specify timestep
68   timestep  0.001
69
70   #####
71   #ENERGY EVALUATION
72   thermo_style  custom step temp press pe ke etotal
73   thermo 1000
74
75   ##### EQUILIBRATION
76
77   run 1000000
78
79   ##### WRITE EQUILIBRATION RUN BINARY FOR RERUN
80   write_restart restart.equil1
81
82   ##### EXPERIMENT
83   reset_timestep 0
84
85
86   dump  img  all  custom 10000 simulation.snapshot id type xs ys
      zs vx vy vz
87
88   #sample radial distribution function g(r) and save it to lj.
      rdf
89   #the 100 100 10000 means sample every 100 steps, make 100 of
      such samples, and save at 10000 steps
90   compute rdf  all  rdf 250 1 2 2 2 1 1
91   fix saverdf  all  ave/time 100 1000 ${final_step} c_rdf[*]
      file rdf_pack_frac_poly_${phi_poly}_1.dat mode vector
92
93
94   compute tracer_msd mobile msd
95   fix tracer_msd mobile ave/time 2 6 100 c_tracer_msd[4] file
      msd_pack_frac_poly_${phi_poly}.dat
96   compute msd mobile msd
97   thermo_style  custom step temp press pe ke etotal
98   thermo_modify lost error
```

```
99      thermo 1000  
100  
101     run 10000000
```